



HAL
open science

Analysis of a frictional oblique impact observed in skew bridges

Elias G. Dimitrakopoulos

► **To cite this version:**

Elias G. Dimitrakopoulos. Analysis of a frictional oblique impact observed in skew bridges. *Nonlinear Dynamics*, 2009, 60 (4), pp.575-595. 10.1007/s11071-009-9616-7 . hal-00568404

HAL Id: hal-00568404

<https://hal.science/hal-00568404>

Submitted on 23 Feb 2011

HAL is a multi-disciplinary open access archive for the deposit and dissemination of scientific research documents, whether they are published or not. The documents may come from teaching and research institutions in France or abroad, or from public or private research centers.

L'archive ouverte pluridisciplinaire **HAL**, est destinée au dépôt et à la diffusion de documents scientifiques de niveau recherche, publiés ou non, émanant des établissements d'enseignement et de recherche français ou étrangers, des laboratoires publics ou privés.

Analysis of a Frictional Oblique Impact Observed in Skew Bridges

Elias G. Dimitrakopoulos¹

Abstract

The oblique contact/impact of skew bridges triggers a unique rotational mechanism which earthquake reconnaissance reports correlate with deck unseating of such bridges. Building on the work of other researchers, the present study adopts a fully non-smooth rigid body approach and set-valued force laws, in order to analyze in depth this oblique multi-impact phenomenon. A linear complementarity formulation is proposed which yields a great variety of (multi-) impact states, depending on the initial (pre-impact) conditions, such as “slip” or “stick” at one corner (single-impact) or two corners (double-impact) of the body. The pertinent existential conditions of those impact states reveal a complex dynamic behaviour. With respect to the rotational mechanism associated with double-impact, the physically feasible impact states as well as, counter-intuitive exceptions are recognized. The study proves that double oblique impact, both frictionless and frictional, may or may not produce rotation of the body and proposes criteria that distinguish each case. Most importantly, it is shown that the tendency of skew bridges to rotate (and hence unseat) after deck-abutment collisions is not a factor of the skew angle alone, but rather of the overall geometry in-plan, plus the impact parameters (coefficient of restitution and coefficient of friction). The study also provides a theoretical justification of the observed tendency of skew bridges to jam at the obtuse corner and rotate in such a way that the skew angle increases. Finally, counter-intuitive trends hidden in the response are unveiled which indicate that, due to friction, a skew bridge may also rotate so that the skew angle decreases.

Keywords: Oblique Impact, Friction, Unilateral Contact, Complementarity, Skew Bridges, Concrete Bridges

¹Post-doctoral researcher, Dept. of Civil Engineering, Aristotle University of Thessaloniki, Greece, GR 54124

INTRODUCTION

This paper focuses on the impact response of skew bridges with deck-abutment expansion joints, while it belongs to a broader study [1-3] on the problem of the earthquake-induced pounding in (straight and skew) bridges.

Skew bridges exhibit a unique seismic response that is triggered by oblique impact. Earthquake reconnaissance reports [4] indicate that skew bridges often rotate in the horizontal plane, thus tending to drop off the supports at the acute corners [5] (Figure 1). This behaviour results in a coupling of longitudinal and transversal response, binding in one of the obtuse corners and subsequently rotation in the direction of increasing the skew angle [5] (Figure 2).



Figure 1. Damage of a skew bridge after the Tehuacan 1999 Mexico earthquake [6].

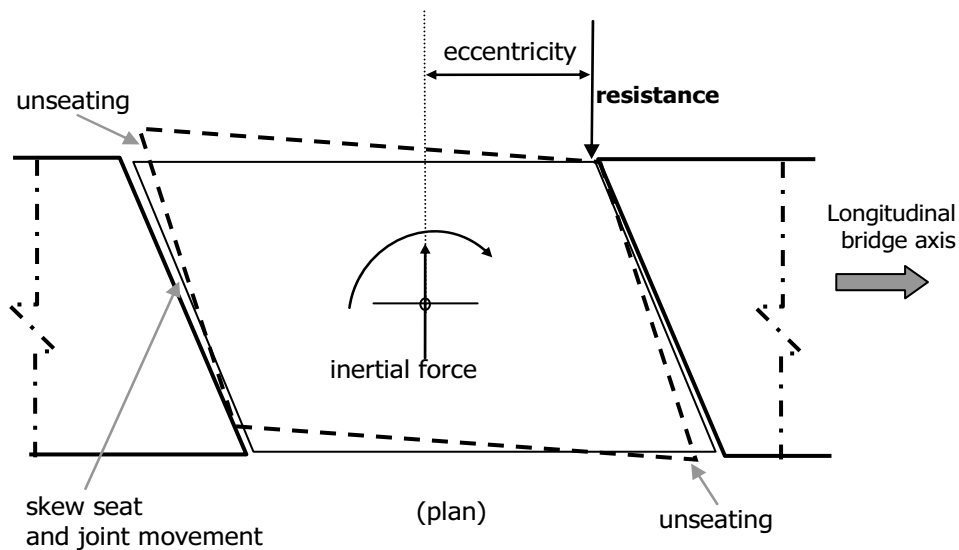


Figure 2. Rotation mechanism of skew bridges – unseating, adopted from [5]

Despite the recorded evidence from previous earthquakes, which underlines the importance of this mechanism, as well as the empirical vulnerability methodologies that acknowledge skew as a primary vulnerability factor in bridges [7], there are only a few attempts to comprehend this mechanism. One of the first was made by Maragakis et al. [8], motivated after the aforementioned type of damage during the 1971 San Fernando earthquake [4]. Maragakis et al. focused on the rigid body motions of a skew bridge, using a rigid stick model of the bridge deck and spring elements to model piers. Pounding with the abutments was simulated with an elastic spring activated after the closure of the gap. More recently, Maleki [9] studied single-span straight and skew bridges using a SDOF model, in an attempt to estimate the forces developed during collision.

In the vast majority of pertinent studies, including the aforementioned ones, impact is considered as centric and is simulated with a contact-element (“compliance” method). However, contact in skew bridges is oblique and multi-point (multi-impact), and disregarding this fact should be attributed to inherent difficulties in properly modelling it. As a consequence, there is a lack of a thorough theoretical investigation, and hence understanding, regarding this peculiarity of skew bridges.

An alternative way to deal with such an impact and investigate in depth the associated rotational mechanism is within the context of non-smooth dynamics. Key feature of this approach, originating from the pioneering studies of Moreau [10] and Panagiotopoulos [11, 12], is the inequality form of the impact laws which often is transformed to linear complementarity. Notions of convex analysis, as well as set – valued (force) laws, have been embedded naturally within this context [13]. In recent years an ever increasing number of structural problems is tackled with the notions of non-smooth dynamics; for instance the seismic behaviour of pounding structures where unilateral contact configurations (impacts, continuous contacts, and detachments) are mathematically treated as inequality problems by Dimitrakopoulos et al. [3].

Within the framework of an event-based methodology [13-15] the seismic response of a bridge can be decomposed into discontinuous events (e.g. impacts) and continuous impact-free motion. Adopting this standpoint, the main gap in the existing knowledge regarding the seismic response of skew bridges is the phenomenon of the aforementioned oblique multi-impact (Figure 2). The key objective of this paper is to fill this gap and at the same time to illustrate the effectiveness of non-smooth

dynamics in a case with practical significance and multidisciplinary interest. The motivation for this study originates from: (i) the need to elucidate the oblique impact response of skew bridges with deck-abutment joints, (ii) the importance of this rotational mechanism manifested by empirical evidence and recognised by empirical vulnerability methodologies for bridges, and (iii) the large number of existing bridges of this type worldwide.

2. PROPOSED METHODOLOGY

In [16] Payr & Glocker re-examined a benchmark problem of impact dynamics illustrating the effectiveness of their non-smooth set-valued approach when compared with more conventional methodologies. The present study builds on the work of Payr & Glocker [16] extending their approach from single to a multiple (double) frictional collision case, which encapsulates a lot of the ‘physics’ of deck-abutment impact in skew bridges. The bridge deck (in-between two successive separation joints) is considered as a rigid body moving in plane and the interaction between deck and abutment is modelled as a unilateral contact.

Herein the most fundamental impact laws are adopted in a set-valued form following [16]. Impact is assumed to behave according to Newton's law in the normal direction and according to Coulomb's friction law in the transversal direction. Hence, only two impact parameters are needed to describe frictional impact, the normal coefficient of restitution ε_N and the coefficient of friction μ . It is reminded that Newton's coefficient of restitution is taken as the ratio of the (relative) contact velocities after, \mathbf{u}^+ , and before, \mathbf{u}^- , impact: $u^+ = -\varepsilon_N u^-$ and it varies between zero and one, $\varepsilon_N \in [0,1]$. In the transversal direction a zero coefficient of restitution is assumed $\varepsilon_T = 0$.

Two set-valued maps, the unilateral primitive (Figure 3 right) and the $Sgn(x)$ function (Figure 3 left) are adopted in the normal, Λ_{Ni} , and the transversal, Λ_{Ti} , direction of impact i , respectively.

$$-\Lambda_{Ni} \in \text{Upr}(v_{Ni}), \quad -\Lambda_{Ti} \in \mu_i \Lambda_{Ni} \text{Sgn}(v_{Ti}) \quad (1)$$

Velocities v_N , v_{TR} and v_{TL} are defined later on with equations (8 to 10).

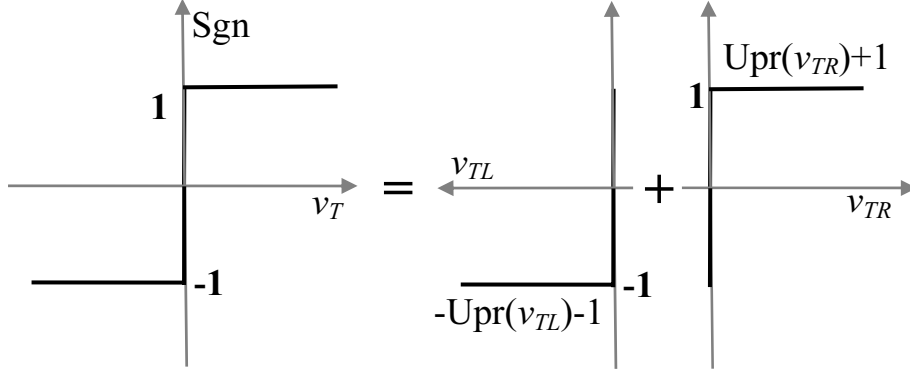


Figure 3. Set-valued friction force law [16].

The $Sgn(x)$ function differs from the standard sgn function, in the point $x = 0$ where the former yields a set of values: $Sgn(x = 0) = [-1, 1]$, instead of a single value $sgn(x=0)=0$. In [16], it is shown that the Sgn function can be decomposed into two unilateral primitives (Figure 3), which is ideal when the problem of impact is formulated as an inequality problem. With the help of Figure 3 the following decomposition can be achieved:

$$\begin{cases} -\Lambda_{TRi} \in \text{Upr}(v_{TRi}) & \Lambda_{TRi} = \mu\Lambda_{Ni} + \Lambda_{Ti} \\ -\Lambda_{TLi} \in \text{Upr}(v_{TLi}) & \Lambda_{TLi} = \mu\Lambda_{Ni} - \Lambda_{Ti} \\ v_{Ti} = v_{TRi} - v_{TLi} \end{cases} \quad (2)$$

or in vector form:

$$\Lambda_{TL} = \bar{\mu}\Lambda_N - \Lambda_T = 2\bar{\mu}\Lambda_N - \Lambda_{TR} \quad (3)$$

where: $\bar{\mu} = \text{diag}\{\mu_i\}$, $\Lambda_N = \{\Lambda_{Ni}\}$, $\Lambda_T = \{\Lambda_{Ti}\}$, $\Lambda_{TL} = \{\Lambda_{TLi}\}$, $\Lambda_{TR} = \{\Lambda_{TRi}\}$.

The problem of frictional multi-impact is formulated herein as a linear complementarity problem (LCP). In the classical form, an LCP is a system of linear equations: $\mathbf{y} = \mathbf{A}\mathbf{x} + \mathbf{b}$, with matrices \mathbf{A} and \mathbf{b} known, and \mathbf{y} and \mathbf{x} the unknown vectors under determination, for which the following additional complementarity conditions hold: $\mathbf{y} \geq 0$, $\mathbf{x} \geq 0$, $\mathbf{y}^T \mathbf{x} = 0$. More details on the LCP as well as an overview of the available algorithms for treating numerically an LCP can be found in [17].

Newton – Euler equations in integrated form, taking into account transversal forces (friction), read as follows:

$$\mathbf{M}(\mathbf{u}^+ - \mathbf{u}^-) = \mathbf{W}_N \Lambda_N + \mathbf{W}_T \Lambda_T \quad (4)$$

where Λ_N and Λ_T are the impulse vectors in the normal and the transversal direction of impact, respectively, \mathbf{M} is the mass matrix and \mathbf{W} are the direction vectors of the

constraints (impact) in the normal (sub-index N) $\mathbf{W}_N = \{\mathbf{w}_{Ni}\}$ and the transversal (sub-index T) $\mathbf{W}_T = \{\mathbf{w}_{Ti}\}$ direction; sub-indexes N, T are used throughout this paper in the same sense. By pre-multiplying with $\mathbf{W}_N^T \mathbf{M}^{-1}$ and $\mathbf{W}_T^T \mathbf{M}^{-1}$, Equation (4) is converted to relative velocities in the normal, $\gamma_{Ni} = \mathbf{w}_{Ni}^T \mathbf{u}$, and the transversal, $\gamma_{Ti} = \mathbf{w}_{Ti}^T \mathbf{u}$, direction of impact, respectively:

$$\begin{aligned}\gamma_N^+ - \gamma_N^- &= \mathbf{W}_N^T \mathbf{M}^{-1} \mathbf{W}_N \Lambda_N + \mathbf{W}_N^T \mathbf{M}^{-1} \mathbf{W}_T \Lambda_T \\ \gamma_T^+ - \gamma_T^- &= \mathbf{W}_T^T \mathbf{M}^{-1} \mathbf{W}_N \Lambda_N + \mathbf{W}_T^T \mathbf{M}^{-1} \mathbf{W}_T \Lambda_T\end{aligned}\quad (5)$$

In Equations (5) and throughout this paper superscript “+” refers to the post-impact state, while super-script “-” to the pre-impact state and $\boldsymbol{\gamma} = \{\gamma_i\}$. Using the notation of Pfeiffer [18]:

$$\begin{aligned}\mathbf{G}_{NN} &= \mathbf{W}_N^T \mathbf{M}^{-1} \mathbf{W}_N & \mathbf{G}_{NT} &= \mathbf{W}_N^T \mathbf{M}^{-1} \mathbf{W}_T \\ \mathbf{G}_{TN} &= \mathbf{W}_T^T \mathbf{M}^{-1} \mathbf{W}_N & \mathbf{G}_{TT} &= \mathbf{W}_T^T \mathbf{M}^{-1} \mathbf{W}_T\end{aligned}\quad (6)$$

Equations (5) are rewritten as:

$$\begin{aligned}\gamma_N^+ - \gamma_N^- &= \mathbf{G}_{NN} \Lambda_N + \mathbf{G}_{NT} \Lambda_T \\ \gamma_T^+ - \gamma_T^- &= \mathbf{G}_{TN} \Lambda_N + \mathbf{G}_{TT} \Lambda_T\end{aligned}\quad (7)$$

The following velocity jumps are defined:

$$\begin{aligned}\mathbf{v}_N &\doteq \boldsymbol{\gamma}_N^+ + \bar{\bar{\varepsilon}}_N \boldsymbol{\gamma}_N^- \\ \mathbf{v}_T &\doteq \boldsymbol{\gamma}_T^+ = \mathbf{v}_{TR} - \mathbf{v}_{TL}\end{aligned}\quad (8)$$

In the normal direction of the impact, it holds that:

$$\left. \begin{aligned}\mathbf{v}_N &\doteq \boldsymbol{\gamma}_N^+ + \bar{\bar{\varepsilon}}_N \boldsymbol{\gamma}_N^- \\ \boldsymbol{\gamma}_N^+ &= \boldsymbol{\gamma}_N^- + \mathbf{G}_{NN} \Lambda_N + \mathbf{G}_{NT} \Lambda_T \\ \Lambda_T &= \Lambda_{TR} - \bar{\bar{\mu}} \Lambda_N\end{aligned}\right\} \Rightarrow \mathbf{v}_N = (\mathbf{G}_{NN} - \mathbf{G}_{NT} \bar{\bar{\mu}}) \Lambda_N + \mathbf{G}_{NT} \Lambda_{TR} + (\bar{\bar{\varepsilon}}_N + \mathbf{E}) \boldsymbol{\gamma}_N^- \quad (9)$$

Similarly in the transversal direction:

$$\left. \begin{aligned}\mathbf{v}_T &= \mathbf{v}_{TR} - \mathbf{v}_{TL} \\ \boldsymbol{\gamma}_T^+ &= \boldsymbol{\gamma}_T^- + \mathbf{G}_{TN} \Lambda_N + \mathbf{G}_{TT} \Lambda_T \\ \Lambda_T &= \Lambda_{TR} - \bar{\bar{\mu}} \Lambda_N\end{aligned}\right\} \Rightarrow \mathbf{v}_{TR} = (\mathbf{G}_{TN} - \mathbf{G}_{TT} \bar{\bar{\mu}}) \Lambda_N + \mathbf{G}_{TT} \Lambda_{TR} + \mathbf{E} \boldsymbol{\gamma}_T^- + \mathbf{v}_{TL} \quad (10)$$

Where: $\bar{\bar{\mu}} = \text{diag}\{\mu_i\}$, $\bar{\bar{\varepsilon}}_N = \text{diag}\{\varepsilon_{Ni}\}$, i is the index of the impact points, \mathbf{E} the identity matrix, and μ , ε_N , the coefficients of friction and restitution respectively.

From Equations (6) to (10) an LCP is formulated that treats a frictional multi-impact:

$$\begin{pmatrix} \mathbf{v}_N \\ \mathbf{v}_{TR} \\ \boldsymbol{\Lambda}_{TL} \end{pmatrix} = \begin{pmatrix} \mathbf{G}_{NN} - \mathbf{G}_{NT}\bar{\mu} & \mathbf{G}_{NT} & \mathbf{0} \\ \mathbf{G}_{TN} - \mathbf{G}_{TT}\bar{\mu} & \mathbf{G}_{TT} & \mathbf{E} \\ 2\bar{\mu} & -\mathbf{E} & \mathbf{0} \end{pmatrix} \begin{pmatrix} \boldsymbol{\Lambda}_N \\ \boldsymbol{\Lambda}_{TR} \\ \mathbf{v}_{TL} \end{pmatrix} + \begin{pmatrix} (\bar{\varepsilon}_N + \mathbf{E})\boldsymbol{\gamma}_N^- \\ \mathbf{E}\boldsymbol{\gamma}_T^- \\ \mathbf{0} \end{pmatrix} \quad (11)$$

$$\begin{pmatrix} \mathbf{v}_N \\ \mathbf{v}_{TR} \\ \boldsymbol{\Lambda}_{TL} \end{pmatrix} \geq \mathbf{0}, \begin{pmatrix} \boldsymbol{\Lambda}_N \\ \boldsymbol{\Lambda}_{TR} \\ \mathbf{v}_{TL} \end{pmatrix} \geq \mathbf{0}, \begin{pmatrix} \mathbf{v}_N \\ \mathbf{v}_{TR} \\ \boldsymbol{\Lambda}_{TL} \end{pmatrix}^T \begin{pmatrix} \boldsymbol{\Lambda}_N \\ \boldsymbol{\Lambda}_{TR} \\ \mathbf{v}_{TL} \end{pmatrix} = 0 \quad (12)$$

As illustrated in later sections, in the form of Equations (11 and 12) the formulated LCP yields a great variety of solutions and is capable of encapsulating different impact states such as “slip”, “stick” and reversal of sign, both for single-impact [16] and for double-impact, and contains also impacts of non-impulsive behaviour. The adopted approach is thus set-valued and non-smooth in contrast to the commonly adopted, in earthquake engineering literature, contact-element approach (see for example references in [3]). The main difference with the pertinent LCP of [16] that treats single collisions, is that all elements of the LCP (Equation 11) are, in the general case, matrices instead of scalar quantities. Similar LCP formulations problems have been proposed in the past among others by Kwack & Lee [19] and Klarbring & Bjrrkman [20]. The proposed LCP formulation (Equations 11 and 12) though, is very well - suited for the needs of the present analysis which is confined to analytical solutions.

3 GEOMETRIC CONSIDERATIONS

3.1 The Kinematic Part of the Impact Problem

The kinematic part of the impact problem consists in expressing the relative distances g_i (gap functions) and the corresponding velocities $\dot{\gamma}_i$ of the (potential) impact points i as a function of the generalised coordinates q_i . The generalised coordinate vector is comprised by the (three) degrees of freedom of a rigid body in plan: two translational (x, y) along the two horizontal axes and one rotational (θ) around the vertical axis; $\mathbf{q}^T = [x \ y \ \theta]$. The pertinent velocities are given by $\dot{\mathbf{q}} = \mathbf{u} = (u_x, u_y, u_\theta)^T$.

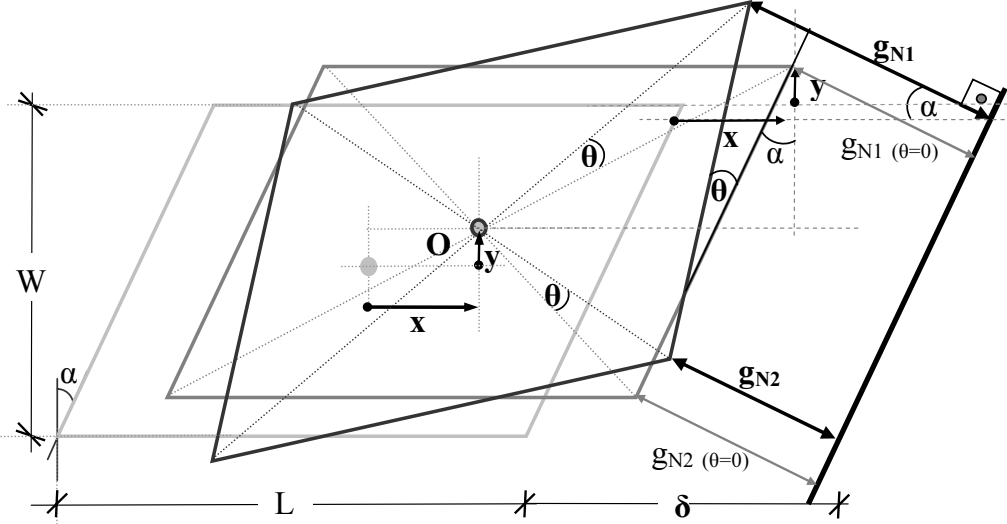


Figure 4. Relative distance of the two potential impact points for planar translational and rotational motion of a skew bridge segment (rigid body). Light grey line - initial position, dark grey line – position after translational motion, black line – position after rotation.

Figure 4 presents a skew bridge segment (rigid body) moving in plan against a rigid barrier, which herein is considered as an inelastic half-space. The relative distance of the two potential impact points g_{N1} , g_{N2} can be derived, after some geometric considerations, as:

$$\begin{aligned} g_{N1} &= (\delta - x) \cos \alpha + y \sin \alpha + \frac{1}{2} [L \cos a (1 - \cos \theta) + (W / \cos a + L \sin a) \sin \theta] \\ g_{N2} &= (\delta - x) \cos \alpha + y \sin \alpha - \frac{1}{2} [L \cos a (\cos \theta - 1) + (W / \cos a - L \sin a) \sin \theta] \end{aligned} \quad (13)$$

where δ is the gap width, α the skew angle, L the length and W the width of the rigid body respectively. In order to shorten the equations, the following notations are introduced:

$$\begin{aligned} c a &= \cos a, \quad s a = \sin a & r_T &= L c a / 2 \\ r_1 &= (L s a + W / c a) / 2 & r_2 &= (L s a - W / c a) / 2 \\ \tilde{r}_{N1} &= \frac{1}{2} [L c a \sin \theta + 2 r_1 \cos \theta] & \tilde{r}_{N2} &= \frac{1}{2} [L c a \sin \theta + 2 r_2 \cos \theta] \\ \tilde{r}_{T1} &= \frac{1}{2} [-2 r_1 \sin \theta + L c a \cos \theta] & \tilde{r}_{T2} &= \frac{1}{2} [2 r_2 \sin \theta + L c a \cos \theta] \end{aligned} \quad (14)$$

Quantities r_1 , r_2 , and r_T , are the lever arms of the pertinent impulses Λ_1 and Λ_2 with respect to the centre of mass, under the assumption of small deformations (see Figure 6 later on). Quantities \tilde{r}_{N1} , \tilde{r}_{N2} , \tilde{r}_{T1} , \tilde{r}_{T2} are the corresponding lever arms in the normal and the transversal direction of the two impacts for large deformations, it follows that: $\tilde{r}_{Ni} \xrightarrow{(\theta \rightarrow 0)} r_i$ and $\tilde{r}_{Ti} \xrightarrow{(\theta \rightarrow 0)} r_T$ where $i = 1, 2$.

The relative velocities of the two impacts in the longitudinal direction, γ_{N1} and γ_{N2} , are calculated by differentiating in time the expressions of g_{N1} and g_{N2} (Equations 13). In the transversal direction the relative velocities, γ_{T1} and γ_{T2} , are derived similarly after calculating the distance variation (e.g. from the initial position – light grey line) due to translational (dark grey line) and rotational (black line) motion with the help of Figure 4.

$$\begin{aligned} \gamma_{N1} &= \underbrace{\begin{pmatrix} -ca & sa & \tilde{r}_{N1} \end{pmatrix}}_{\mathbf{w}_{N1}^T} \underbrace{\begin{pmatrix} u_x \\ u_y \\ u_\theta \end{pmatrix}}_{\mathbf{u}}, & \gamma_{N2} &= \underbrace{\begin{pmatrix} -ca & sa & \tilde{r}_{N2} \end{pmatrix}}_{\mathbf{w}_{N2}^T} \underbrace{\begin{pmatrix} u_x \\ u_y \\ u_\theta \end{pmatrix}}_{\mathbf{u}} \\ \gamma_{T1} &= \underbrace{\begin{pmatrix} sa & ca & \tilde{r}_{T1} \end{pmatrix}}_{\mathbf{w}_{T1}^T} \underbrace{\begin{pmatrix} u_x \\ u_y \\ u_\theta \end{pmatrix}}_{\mathbf{u}}, & \gamma_{T2} &= \underbrace{\begin{pmatrix} sa & ca & \tilde{r}_{T2} \end{pmatrix}}_{\mathbf{w}_{T2}^T} \underbrace{\begin{pmatrix} u_x \\ u_y \\ u_\theta \end{pmatrix}}_{\mathbf{u}} \end{aligned} \quad (15)$$

3.2 Impact Types Considered

In skew bridges with deck-abutment joints, impact in plan can take place either in a corner, single (point) impact or along a side multi (point) impact. In order to cover all potential impact types, from a geometrical point of view, the following cases are distinguished: single-impact (Figure 5 left) and multi-impact (Figure 5 right).

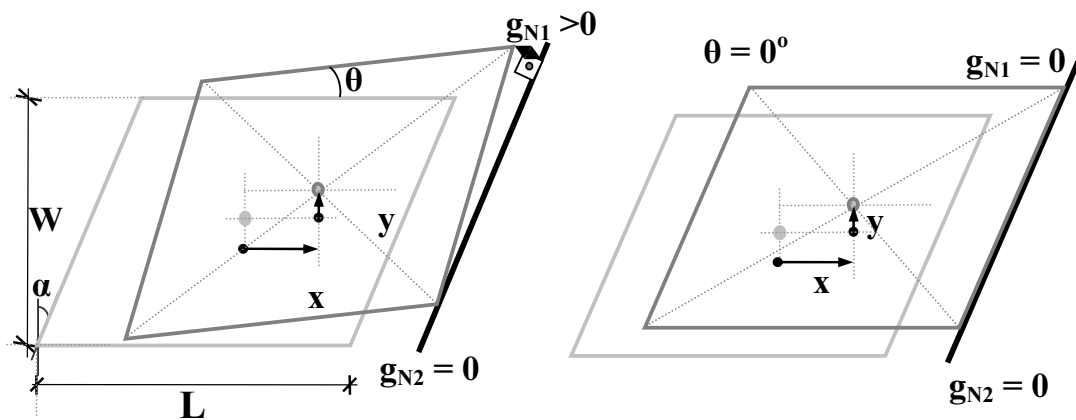


Figure 5. Single-impact (left), and multi-impact (right) of a planar skew rigid body.

4 FRICTIONLESS IMPACT

4.1 Single frictionless impact

Firstly, the case of frictionless impact is discussed without referring to the LCP (11). The effective mass during collision, in the normal direction, G_{NN}^{-1} [21], is calculated as:

$$G_{NN} \doteq \frac{1}{m} + \tilde{r}_N^2 \frac{1}{I_m}, \quad G_{NN}^{-1} = \frac{mI_m}{I_m + \tilde{r}_N^2 m} \quad (16)$$

where lever arm \tilde{r}_N is taken as $\tilde{r}_N = \tilde{r}_{N1}$ or \tilde{r}_{N2} depending on the examined corner where impact takes place and I_m is the inertial mass. The impulse vector Λ_N can be estimated according to the assumed impact law, herein Newton's law [21]:

$$\Lambda_N = -\mathbf{G}_{NN}^{-1} (\mathbf{E} + \bar{\bar{\epsilon}}_N) \gamma_N^- \quad (17)$$

where \mathbf{E} , is the identity matrix and $\bar{\bar{\epsilon}}_N = \text{diag} \{ \epsilon_{Ni} \}$ the diagonal matrix comprised by the coefficients of restitution of impacts i .

In the case of single-impact (Figure 5 left), Equation (17) simplifies to:

$$\Lambda_N = (1 + \epsilon_N) \frac{-mI_m}{I_m + \tilde{r}_N^2 m} \underbrace{(-c a \cdot u_x^- + s a \cdot u_y^- + \tilde{r} \cdot u_\theta^-)}_{\gamma_N^-} \Leftrightarrow \frac{\Lambda_N}{m \gamma_N^-} = - \frac{1 + \epsilon_N}{1 + \frac{\tilde{r}_N^2}{\rho^2}} \quad (18)$$

ρ is the radius of gyration, defined from $\rho^2 = I_m/m$

4.2 Multiple frictionless impact

Full-edge impact is modeled (and referred to) as double - impact due to rigid body assumption. Double - impact occurs (Figure 5 right) when $\theta=0$ and $u_\theta^- = 0$. Note that pre-impact velocities u_x^- , u_y^- are kept arbitrary. In this case matrix \mathbf{G}_{NN} and its inverse \mathbf{G}_{NN}^{-1} are as follows:

$$\mathbf{G}_{NN} \doteq \begin{pmatrix} \frac{1}{m} + r_1^2 \frac{1}{I_m} & \frac{1}{m} + r_1 r_2 \frac{1}{I_m} \\ \frac{1}{m} + r_2 r_1 \frac{1}{I_m} & \frac{1}{m} + r_2^2 \frac{1}{I_m} \end{pmatrix}, \quad \mathbf{G}_{NN}^{-1} = \frac{1}{(r_1 - r_2)^2} \begin{pmatrix} I_m + r_2^2 m & -I_m - r_1 r_2 m \\ -I_m - r_2 r_1 m & I_m + r_1^2 m \end{pmatrix} \quad (19)$$

In order to determine the unknown generalized velocities after impact, \mathbf{u}^+ , one has to calculate first the corresponding impulses Λ_N . With the aid of Newton's impact law (Equation 17) it follows that:

$$\Lambda_N = \begin{pmatrix} \Lambda_{N1} \\ \Lambda_{N2} \end{pmatrix} = \frac{-\gamma_N^-}{(r_1 - r_2)^2} \begin{pmatrix} I_m (\varepsilon_{N1} - \varepsilon_{N2}) + m (r_2^2 + r_2^2 \varepsilon_{N1} - r_1 r_2 - r_1 r_2 \varepsilon_{N2}) \\ I_m (-\varepsilon_{N1} + \varepsilon_{N2}) + m (-r_1 r_2 - r_1 r_2 \varepsilon_{N1} + r_1^2 + r_1^2 \varepsilon_{N2}) \end{pmatrix} \quad (20)$$

Assuming the coefficients of restitution in the two impacts ε_{N1} , ε_{N2} are the same $\varepsilon_{N1} = \varepsilon_{N2} = \varepsilon_N$ Equation (20) yields:

$$\begin{pmatrix} \frac{\Lambda_{N1}}{m\gamma_N^-} \\ \frac{\Lambda_{N2}}{m\gamma_N^-} \end{pmatrix} = -(1 + \varepsilon_N) \begin{pmatrix} -\frac{r_2}{r_1 - r_2} \\ \frac{r_1}{r_1 - r_2} \end{pmatrix} = -\frac{(1 + \varepsilon_N)}{2} \begin{pmatrix} 1 - \frac{\sin a \cos a}{W/L} \\ 1 + \frac{\sin a \cos a}{W/L} \end{pmatrix} \quad (21)$$

Using Equations (4) the unknown generalized velocities after impact \mathbf{u}^+ are calculated as:

$$\mathbf{u}^+ = \mathbf{u}^- - \mathbf{M}^{-1} \mathbf{W}_N \underbrace{\mathbf{G}_N^{-1} (\mathbf{E} + \bar{\bar{\mathbf{e}}}_N)}_{-\Lambda_N} \gamma^- \Rightarrow \begin{pmatrix} u_x^+ \\ u_y^+ \\ u_\theta^+ \end{pmatrix} = \begin{pmatrix} u_x^- \\ u_y^- \\ 0 \end{pmatrix} + \begin{pmatrix} -\frac{ca}{m} \Lambda_{N1} - \frac{ca}{m} \Lambda_{N2} \\ \frac{sa}{m} \Lambda_{N1} + \frac{sa}{m} \Lambda_{N2} \\ \frac{r_1}{I_m} \Lambda_{N1} + \frac{r_2}{I_m} \Lambda_{N2} \end{pmatrix} \quad (22)$$

From Equations (22), due to (21), it follows that the post-impact angular velocity is zero, $u_\theta^+ = 0$.

Impulses Λ_{N1} and Λ_{N2} are given by Equations (21) as a function of the geometry (α, L, W), the coefficient of restitution in the normal direction ε_N , and the translational mass m . However, Equations (21) are incomplete without the physical inequality constraint $\Lambda_N \geq 0$ which accounts for the unilateral nature of impact. Unlike single-impact (Equation 18), in multi-impacts the satisfaction of the inequality constraint demands special attention [21].

Indeed, taking into account that by definition: $m(1 + \varepsilon_N) > 0$, and that in order for contact to occur the relative velocity must be negative $\gamma_N^- \leq 0$ (approach process), the sign of impulse depends solely on the (proposed) dimensionless criterion, η_0 , which relates the ratio of the two sides in plan (L, W) with the skew angle, α , as follows:

$$\eta_0 = \frac{\sin 2\alpha}{2(W/L)} \quad (23)$$

For $\eta_0 > 1$, impulse at the acute corner according to Equations (21) is negative $\Lambda_{N1} < 0$, which lacks physical interpretation. On the contrary, impulse at the obtuse corner is always positive, $\Lambda_{N2} > 0$ (Equations 21).

As mentioned previously, no angular velocity is developed after the examined oblique impact (Figure 5 right) and thus rotation remains zero, $u_\theta^+ = 0$, as assumed before impact. This not so intuitive conclusion though, is valid only when constraint $A_N \geq 0$ is satisfied or equivalently when $\eta_0 < 1$ (Figure 6 top). If $\eta_0 > 1$ (Figure 6 bottom), contact at the acute corner must be ignored (since $A_{N1} < 0$) and Equations (22) of the multi-impact have to be replaced by Equation (18), assuming single-impact solely at the obtuse corner. In summary, the generalised angular velocity, u_θ^+ , after double impact is given by:

$$u_\theta^+ = \begin{cases} \frac{\gamma_N^-}{r_2} \frac{1 + \varepsilon_N}{\left(\frac{\rho}{r_2}\right)^2 + 1}, & \text{if } \eta_0 = \frac{\sin 2\alpha}{2(W/L)} > 1 \\ 0, & \text{if } \eta_0 = \frac{\sin 2\alpha}{2(W/L)} < 1 \end{cases} \quad (24)$$

Equations (24) unveil two distinct response patterns of a planar skew body after double oblique impact. When $\eta_0 < 1$, or equivalently $W/\cos\alpha > L\sin\alpha$ (Figure 6 top), the angular momentums of the two impulses A_{N1} and A_{N2} with respect to the centre of mass (C.M.) are in different directions and cancel out, as a consequence no angular velocity is developed (Equations 24). On the contrary, when $\eta_0 > 1$, subsequently $W/\cos\alpha < L\sin\alpha$ (Figure 6 bottom) the angular momentums of the two impulses A_{N1} and A_{N2} are in the same direction, the impulse at the acute corner should then be neglected since according to Equation (21) it changes sign ($A_{N1} < 0$) and angular velocity is developed (Equation 24). This behaviour of a skew rigid body after double oblique impact reminiscents the behaviour of the double impact of a rod [21].

To date, these two distinct response patterns of deck-abutment collisions of skew bridges were not known. Furthermore, Equations (24) reveal that the tendency of such bridges towards rotation (and most importantly unseating) is not a factor of the skew angle (α) alone, as considered in empirical vulnerability methodologies e.g. [7] but rather of the overall geometry of the body in-plan (criterion η_0 Equation 23). Figure 7 plots contours of the dimensionless criterion η_0 on the plane: Width and Length ratio (W/L) vs. Skew angle (α). Every point on this plane shapes the form of a skew bridge segment in plan. For example, small α and W/L ratio around unity correspond to a square body (Figure 7 top left, $\eta_0 \approx 0.2$) while large α and low W/L ratios to a bridge like the one at the bottom right of Figure 7 ($\eta_0 \approx 2.0$). Figure 7 also

shows that a bridge with a smaller skew angle (α) is feasible to yield a greater dimensionless skew value (η_0) than one with a larger skew angle.

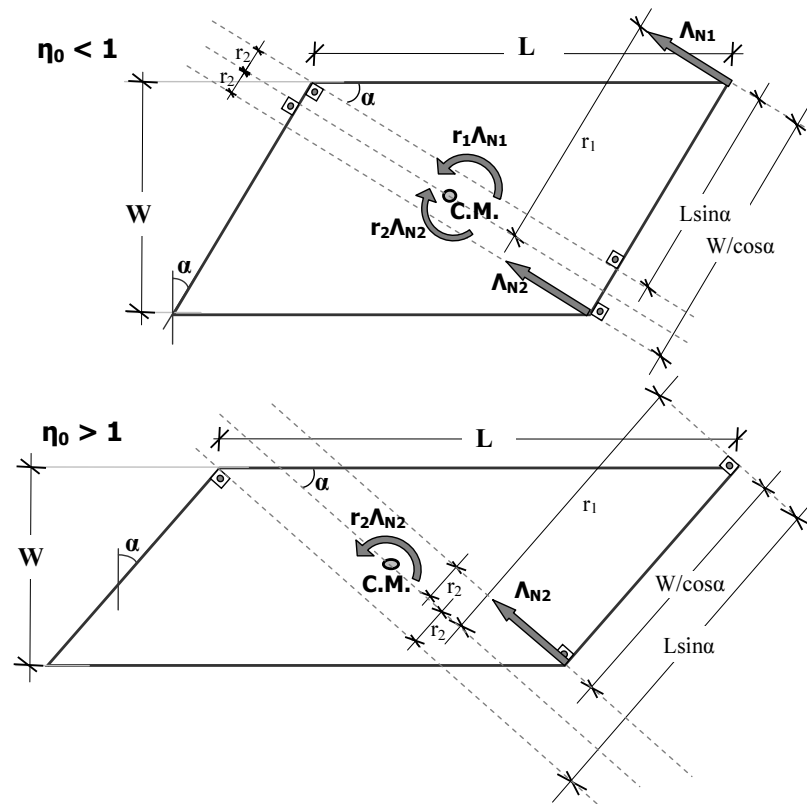


Figure 6. Geometrical interpretation of the rotational mechanism of skew bridges (frictionless impact). Top: no rotation is developed after double-impact. Bottom: double-impact results in rotation.

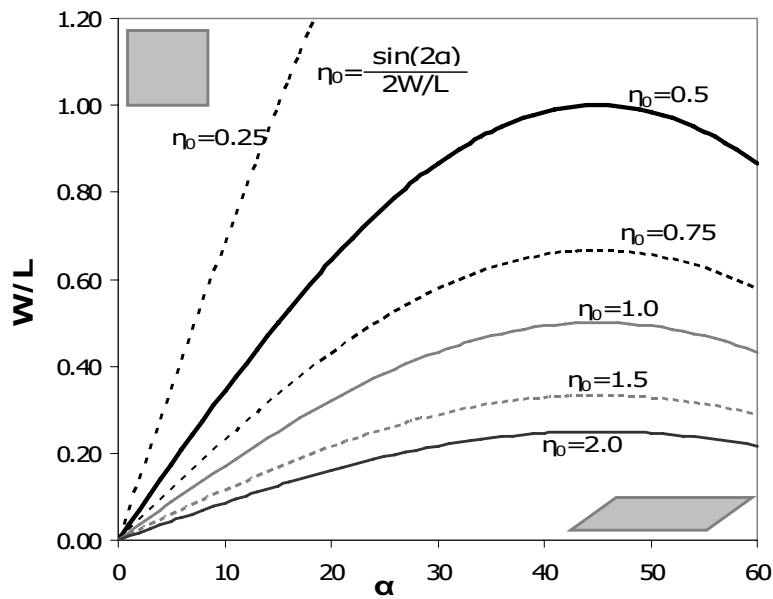


Figure 7. Contours of the dimensionless skew criterion η_0 values in the plane: Width/Length (W/L) – Skew angle (α).

5 FRICTIONAL IMPACT

A more realistic description of the oblique impact response of skew bridges is obtained when friction is taken into account. However, the ad hoc method, of checking the sign of the impulse a-posteriori used in the previous section, is inappropriate for complicated (such as multi-frictional) impact configurations [16, 21]. Instead, a more effective method is to formulate the impact problem taking into account the unilateral character of contact from the beginning, for instance by means of a Linear Complementarity Problem (LCP, Equations 11 and 12).

The LCP (11) with the complementarity conditions (12) yields a great variety of solutions. In addition to the single-impact states investigated in [16] three multi-impact states appear: double backward slip (Figure 8 top), double forward slip (Figure 8 bottom) and double stick (Figure 9 later on). It is reminded that in the transversal direction a Coulomb friction model is realized via a set-value force law; the $Sgn(x)$ function (Figure 3).

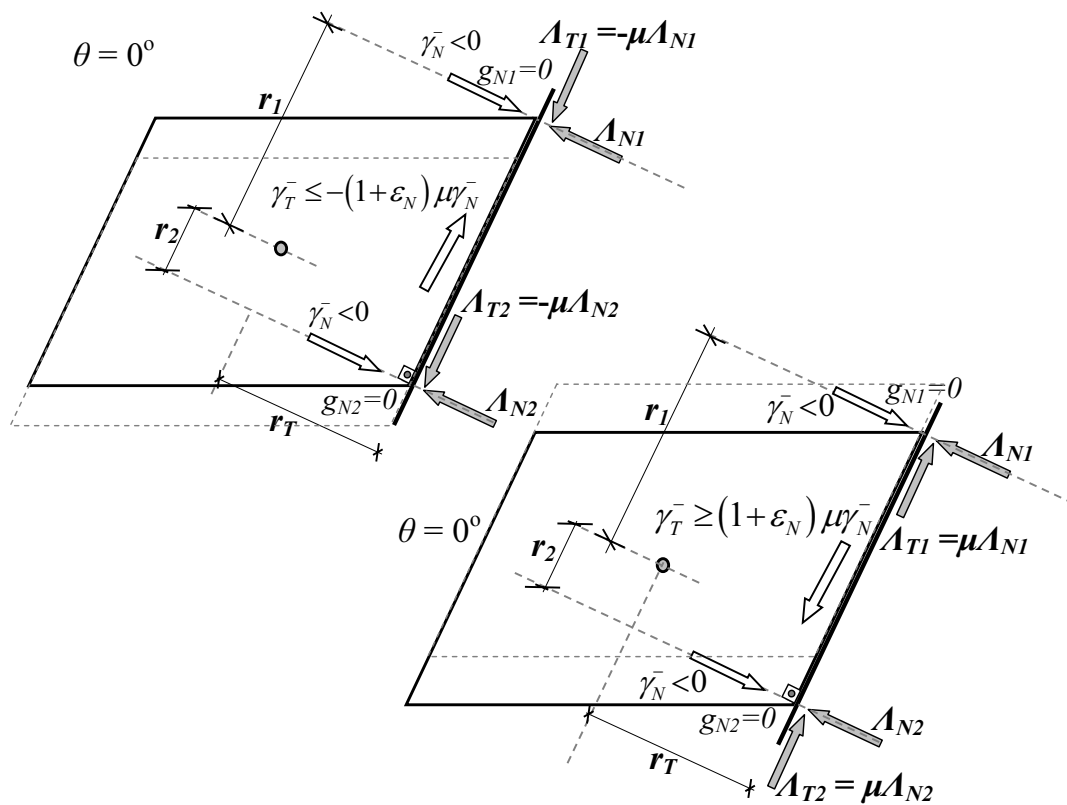


Figure 8. Double backward slip (top), double forward slip (bottom)

5.1 Multiple frictional impact states

The discussion of frictional impact begins with double-impact. Later in the paper, it is shown that for the mechanical configuration considered herein, single-impact states can be seen as a special case of the double-impact examined. Double-impact occurs when $u_{\theta}^- = 0$ and $\theta^- = 0$ (Figure 5 right).

Firstly, \mathbf{G} - matrices are calculated according to Equations (6):

$$\begin{aligned} \mathbf{G}_{NN} &= \begin{pmatrix} \frac{1}{m} + \frac{r_1^2}{I_m} & \frac{1}{m} + \frac{r_1 r_2}{I_m} \\ \frac{1}{m} + \frac{r_1 r_2}{I_m} & \frac{1}{m} + \frac{r_2^2}{I_m} \end{pmatrix} & \mathbf{G}_{NT} &= \begin{pmatrix} \frac{r_1 r_T}{I_m} & \frac{r_1 r_T}{I_m} \\ \frac{r_2 r_T}{I_m} & \frac{r_2 r_T}{I_m} \end{pmatrix} \\ \mathbf{G}_{TT} &= \begin{pmatrix} \frac{1}{m} + \frac{r_T^2}{I_m} & \frac{1}{m} + \frac{r_T^2}{I_m} \\ \frac{1}{m} + \frac{r_T^2}{I_m} & \frac{1}{m} + \frac{r_T^2}{I_m} \end{pmatrix} & \mathbf{G}_{TN} &= \begin{pmatrix} \frac{r_1 r_T}{I_m} & \frac{r_2 r_T}{I_m} \\ \frac{r_1 r_T}{I_m} & \frac{r_2 r_T}{I_m} \end{pmatrix} \end{aligned} \quad (25)$$

The inverse of matrix \mathbf{G}_{NN} expresses the effective mass in the normal direction of the impact [21] and is given by:

$$\mathbf{G}_{NN}^{-1} = \frac{1}{(r_1 - r_2)^2} \begin{pmatrix} I_m + r_2^2 m & -I_m - r_1 r_2 m \\ -I_m - r_2 r_1 m & I_m + r_1^2 m \end{pmatrix} \quad (26)$$

On the contrary, matrices \mathbf{G}_{NT} , \mathbf{G}_{TT} and \mathbf{G}_{TN} are not invertible since determinants: $|\mathbf{G}_{NT}| = |\mathbf{G}_{TT}| = |\mathbf{G}_{TN}| = 0$ are zero. This is a typical case of dependent constraints which arises because the two impacts are linearly interdependent in the transversal direction. Such *overconstrained* problems appear often in multibody dynamics with multi-impacts and several ways of treating them have been proposed in the literature [14].

I. Double backward slip (Figure 8 top)

The complementarity conditions (12) for $\Lambda_{N1} > 0$, $\Lambda_{N2} > 0$, $\Lambda_{T1} = +\mu\Lambda_{N1}$ and $\Lambda_{T2} = +\mu\Lambda_{N2}$ yield: $v_{N1} = 0$, $v_{N2} = 0$, $\Lambda_{TR1} = 2\mu\Lambda_{N1}$, $v_{TR1} = 0$, $\Lambda_{TR2} = 2\mu\Lambda_{N2}$ and $v_{TR2} = 0$. Thus, Equation (9) reduces to:

$$(\mathbf{G}_{NN} + \mathbf{G}_{NT}\bar{\mu})\Lambda_N = -(\bar{\varepsilon}_N + \mathbf{E})\gamma_N^- \quad (27)$$

The inverse of matrix $(\mathbf{G}_{NN} + \mathbf{G}_{NT}\bar{\mu})$ is given by:

$$(\mathbf{G}_{NN} + \mathbf{G}_{NT}\bar{\bar{\mu}})^{-1} = \frac{1}{(r_1 - r_2)^2} \begin{pmatrix} \mathbf{I}_m + m(r_2^2 + \mu r_2 r_T) & -\mathbf{I}_m - m(r_1 r_2 + \mu r_1 r_T) \\ -\mathbf{I}_m - m(r_1 r_2 + \mu r_2 r_T) & \mathbf{I}_m + m(r_1^2 + \mu r_1 r_T) \end{pmatrix} \quad (28)$$

Note that for $\mu = 0$ Equation (28) reduces to Equation (19) of frictionless collisions. The impulse vector is derived from Equation (27) due to (28) as:

$$\begin{pmatrix} \frac{\Lambda_{N1}}{m\gamma_N^-} \\ \frac{\Lambda_{N2}}{m\gamma_N^-} \end{pmatrix} = -(1 + \varepsilon_N) \begin{pmatrix} \frac{-r_2 - \mu r_T}{r_1 - r_2} \\ \frac{r_1 + \mu r_T}{r_1 - r_2} \end{pmatrix} \quad (29)$$

Equation (10), replacing Λ_N from (29), becomes:

$$\mathbf{v}_{TL} = (\mathbf{G}_{TN} + \mathbf{G}_{TT}\bar{\bar{\mu}})(\mathbf{G}_{NN} + \mathbf{G}_{NT}\bar{\bar{\mu}})^{-1} (\bar{\bar{\varepsilon}}_N + \mathbf{E})\gamma_N^- - \mathbf{E}\gamma_T^- \quad (30)$$

The product $(\mathbf{G}_{TN} + \mathbf{G}_{TT}\bar{\bar{\mu}})(\mathbf{G}_{NN} + \mathbf{G}_{NT}\bar{\bar{\mu}})^{-1}$ after some algebra simplifies to:

$$(\mathbf{G}_{TN} + \mathbf{G}_{TT}\bar{\bar{\mu}})(\mathbf{G}_{NN} + \mathbf{G}_{NT}\bar{\bar{\mu}})^{-1} = \begin{pmatrix} -\frac{\mu r_2 - r_T}{r_1 - r_2} & \frac{\mu r_1 - r_T}{r_1 - r_2} \\ -\frac{\mu r_2 - r_T}{r_1 - r_2} & \frac{\mu r_1 - r_T}{r_1 - r_2} \end{pmatrix} \quad (31)$$

Replacing (31) in Equation (30) shows that the transversal post-impact velocities of the two impact points, in the case of double backward slip, are equal:

$$\gamma_{T1}^+ = \gamma_{T2}^+, \quad \frac{\gamma_{T1}^+}{\gamma_N^+} = -\frac{1 + \varepsilon_N}{\varepsilon_N} \mu + \frac{1}{\varepsilon_N} \frac{\gamma_T^-}{\gamma_N^-} \quad (32)$$

According to Newton – Euler equations double backward slip results in zero angular velocity, since:

$$\begin{aligned} \mathbf{M}(\mathbf{u}^+ - \mathbf{u}^-) &= \mathbf{W}_N \Lambda_N + \mathbf{W}_T \Lambda_T \Rightarrow \\ I_m (u_\theta^+ - 0) &= r_1 \Lambda_{N1} + r_2 \Lambda_{N2} + r_T (\Lambda_{T1} + \Lambda_{T2}) = 0 \Rightarrow u_\theta^+ = 0 \end{aligned}$$

Double backward slip, (Figure 8 top) occurs when: $(\Lambda_N \quad \Lambda_{TR} \quad \mathbf{v}_{TL})^T \geq 0 \Rightarrow (\Lambda_{N1} \quad \Lambda_{N2} \quad \Lambda_{TR1} \quad \Lambda_{TR2} \quad v_{TL1} \quad v_{TL2})^T \geq 0$, which with the help of the LCP (11) yield two existential conditions:

$$\Lambda_{N1} \geq 0 \Rightarrow r_2 + \mu r_T \leq 0 \Rightarrow \eta_1 \leq 1, \quad \text{where } \eta_1 \doteq \eta_0 \left(1 + \frac{\mu}{\tan a} \right) \quad (33)$$

$$\mathbf{v}_{TL} \geq 0 \Rightarrow \frac{\gamma_{T1}^-}{\gamma_N^-} \geq (1 + \varepsilon_N) \mu, \quad \text{and } \gamma_{T1}^- = \gamma_{T2}^- \quad (34)$$

II. Double forward slip (Figure 8 bottom)

Following the same reasoning for forward slip ($\Lambda_{N1} > 0$, $\Lambda_{N2} > 0$, $\Lambda_{T1} = -\mu\Lambda_{N1}$ and $\Lambda_{T2} = -\mu\Lambda_{N2}$), as for double backward slip, the normal impulse vector, $\Lambda_{\mathbf{N}}$ is given by:

$$\begin{pmatrix} \frac{\Lambda_{N1}}{m\gamma_N^-} \\ \frac{\Lambda_{N2}}{m\gamma_N^-} \end{pmatrix} = -(1 + \varepsilon_N) \begin{pmatrix} \frac{-r_2 + \mu r_T}{r_1 - r_2} \\ \frac{r_1 - \mu r_T}{r_1 - r_2} \end{pmatrix} \quad (35)$$

Equation (10) yields:

$$\mathbf{v}_{TR} = (\mathbf{G}_{TN} - \mathbf{G}_{TT}\bar{\mu})(\mathbf{G}_{NN} - \mathbf{G}_{NT}\bar{\mu})^{-1} (\bar{\varepsilon}_N + \mathbf{E})\gamma_N^- + \mathbf{E}\gamma_T^- \quad (36)$$

and after evaluating the product:

$$(\mathbf{G}_{TN} - \mathbf{G}_{TT}\bar{\mu})(\mathbf{G}_{NN} - \mathbf{G}_{NT}\bar{\mu})^{-1} = \begin{pmatrix} \frac{\mu r_2 + r_T}{r_1 - r_2} & \frac{-\mu r_1 - r_T}{r_1 - r_2} \\ \frac{\mu r_2 + r_T}{r_1 - r_2} & \frac{-\mu r_1 - r_T}{r_1 - r_2} \end{pmatrix} \quad (37)$$

the post-impact velocities of the two impacts are derived:

$$\gamma_{T1}^+ = \gamma_{T2}^+, \quad \frac{\gamma_{T1}^+}{\gamma_N^+} = \frac{1 + \varepsilon_N}{\varepsilon_N} \mu + \frac{1}{\varepsilon_N} \frac{\gamma_T^-}{\gamma_N^-} \quad (38)$$

Similarly to double backward slip, the post-impact angular velocity is zero.

Double forward slip occurs when: $(\Lambda_N \quad \Lambda_{TL} \quad \mathbf{v}_{TR})^T \geq 0$, and with the help of the LCP (11) the following existential conditions are derived:

$$\left. \begin{aligned} \Lambda_{N1} \geq 0 &\Rightarrow \mu r_T \geq r_2 \Rightarrow \eta_0 \left(1 - \frac{\mu}{\tan a}\right) \leq 1 \\ \Lambda_{N2} \geq 0 &\Rightarrow r_1 \geq \mu r_T \Rightarrow \eta_0 \left(\frac{\mu}{\tan a} - 1\right) \leq 1 \end{aligned} \right\} \Rightarrow |\eta_2| \leq 1, \text{ where } \eta_2 \doteq \eta_0 \left(1 - \frac{\mu}{\tan a}\right) \quad (39)$$

$$\mathbf{v}_{TR} \geq 0 \Rightarrow \frac{\gamma_T^-}{\gamma_N^-} \leq (1 + \varepsilon_N) \mu, \text{ and } \gamma_{T1}^- = \gamma_{T2}^- \quad (40)$$

III. Double stick

The complementarity conditions (12) for $\Lambda_{N1} > 0$, $\Lambda_{N2} > 0$, $|\Lambda_{T1}| < \mu\Lambda_{N1}$ and $|\Lambda_{T2}| < \mu\Lambda_{N2}$ yield: $v_{N1} = 0$, $v_{N2} = 0$, $\Lambda_{TR1} > 0$, $\Lambda_{TR2} > 0$, $v_{TR1} = 0$, $v_{TR2} = 0$, $\Lambda_{TL1} > 0$, $\Lambda_{TL2} > 0$, $v_{TL1} = 0$, and $v_{TL2} = 0$. Thus, equations (9) and (10) yield a system of coupled equations that must be solved for both unknown vectors $\Lambda_{\mathbf{N}}$ and $\Lambda_{\mathbf{TR}}$ simultaneously:

$$\begin{aligned} \mathbf{0} &= (\mathbf{G}_{NN} - \mathbf{G}_{NT}\bar{\mu})\Lambda_{\mathbf{N}} + \mathbf{G}_{NT}\Lambda_{\mathbf{TR}} + (\bar{\varepsilon}_N + \mathbf{E})\gamma_N^- \\ \mathbf{0} &= (\mathbf{G}_{TN} - \mathbf{G}_{TT}\bar{\mu})\Lambda_{\mathbf{N}} + \mathbf{G}_{TT}\Lambda_{\mathbf{TR}} + \mathbf{E}\gamma_T^- \end{aligned} \quad (41)$$

As mentioned previously matrices \mathbf{G}_{NT} , \mathbf{G}_{TT} and $(\mathbf{G}_{TN} - \mathbf{G}_{TT}\bar{\mu})$ are not invertible, since the two impacts are dependent (constraints), thus system (41) has no unique solution. In order to derive a closed-form solution for this type of impact (double stick) the problem can be reformulated.

In the case of double stick the post-impact kinematic state of the rigid body is fully determined by definition: $\mathbf{v}_N = \mathbf{0}$ and $\mathbf{v}_T = \mathbf{0}$. This allows the determination of an equivalent single (point) impact that bypasses the problem of overconstrained impacts. With reference to Figure 9 the direction vectors of the equivalent impact are:

$$\mathbf{w}_N^T = (-ca \quad sa \quad r^*) \quad \mathbf{w}_T^T = (sa \quad ca \quad r_T) \quad (42)$$

The only unknown under determination is the lever arm of the single-impact in the normal direction r^* . The Newton – Euler equations for the two simulations of impact (double and equivalent single, Figure 9) give:

$$\mathbf{W}_N \Lambda_N + \mathbf{W}_T \Lambda_T = \mathcal{W}_N \Lambda_N + \mathcal{W}_T \Lambda_T \quad (43)$$

The left-hand side of Equation (43) is the matrix expression of impulse under the assumption of double-impact (Figure 9 top), while the right-hand side the corresponding scalar impulse of the equivalent single-impact (Figure 9 bottom). Since the post-impact kinematic state of the body is known by assumption, it follows that the product $\mathbf{M}(\mathbf{u}^+ - \mathbf{u}^-)$ is also known. After some algebra Equation (43) yields:

$$\begin{aligned} \Lambda_{N1} + \Lambda_{N2} &= \Lambda_N \\ \Lambda_{T1} + \Lambda_{T2} &= \Lambda_T \\ r_1 \Lambda_{N1} + r_2 \Lambda_{N2} &= r^* \Lambda_N \end{aligned} \quad (44)$$

The first two equations of (44) stand for the linear momentum equivalence between the two (double and single) impacts, while the third equation of (44), expresses the equivalence of angular momentums.

The unknown lever of the single-impact, in the normal direction, is given as a function of the pre-impact velocities and the coefficient of restitution from Equations (5) due to (43), after some algebra, as:

$$r^* = -\frac{\Lambda_T}{\Lambda_N} r_T = \frac{-1}{1 + \varepsilon_N} \frac{\gamma_T^-}{\gamma_N^-} r_T \quad (45)$$

Hence introducing condition (45) an equivalent single-impact with the examined double stick may be completely determined a priori.

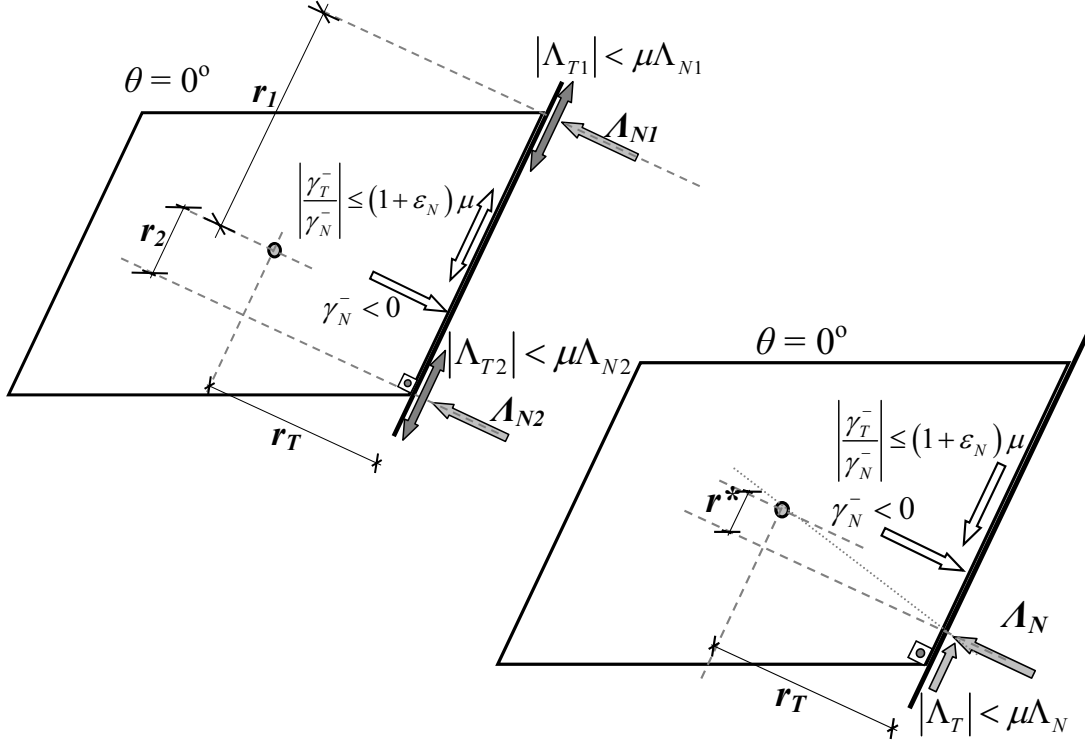


Figure 9. Double stick, simulated as multi-impact (left) and single-impact (right).

In order to derive the existential conditions of double-stick, impulses Λ_{N1} and Λ_{N2} are first calculated from Equation (44) introducing condition (45):

$$\Lambda_{N1} = \frac{r^* - r_2}{r_1 - r_2} \Lambda_N, \quad \Lambda_{N2} = \frac{r_1 - r^*}{r_1 - r_2} \Lambda_N \quad (46)$$

Both Λ_{N1} and Λ_{N2} are positive by assumption, hence:

$$r_1 \geq r^* \geq r_2 \quad (47)$$

Also by assumption, it holds that: $|\Lambda_T| < \mu \Lambda_N$ which due to (45) gives:

$$\left| r^* / r_T \right| \leq \mu \quad (48)$$

as well as:

$$-\mu(1 + \epsilon_N) \leq \frac{\gamma_T^-}{\gamma_N^-} \leq \mu(1 + \epsilon_N) \quad (49)$$

In addition to condition (49) the following existential conditions arise from Equations (47) with the help of Equations (48):

$$\begin{cases} r_2 - \mu r_T < 0 \\ r_1 + \mu r_T > 0 \end{cases} \Rightarrow \begin{cases} \eta_0 (1 - \mu / \tan \alpha) < 1 \\ \eta_0 (1 + \mu / \tan \alpha) > 1 \end{cases} \Rightarrow \begin{cases} \eta_2 < 1 \\ \eta_1 > 1 \end{cases} \quad (50)$$

When $\Lambda_N = 0$ holds at both impact points, double impacts lack physical interpretation. Hence, the remaining physically feasible combinations of the LCP (11) treat double-impact states during which only one of the two impact points presents a compressive impulse ($\Lambda_N > 0$). The comparison of the following impact states with those considered in [16] reveals that these impacts can be treated also with a similar LCP treating single-frictional-impacts.

IV. *Backward slip at the obtuse corner*

Equations (9) and (10) due to the complementarity conditions (12) and $\Lambda_{N2} > 0$, $\Lambda_{N1} = 0$, and $\Lambda_{T2} = +\mu\Lambda_{N2}$ yield:

$$\begin{cases} \frac{\Lambda_{N2}}{m\gamma_N^-} = -\frac{(1+\varepsilon_N)}{1 + \frac{r_2^2 + \mu r_2 r_T}{\rho^2}} \\ \frac{\gamma_{N1}^+}{\gamma_N^-} = 1 + (1+\varepsilon_N) \frac{\rho^2 + r_1 r_2 + \mu r_1 r_T}{\rho^2 + r_2^2 + \mu r_2 r_T} \end{cases} \quad (51)$$

The pertinent existential conditions are:

$$\begin{cases} \Lambda_{N2} \geq 0 \Rightarrow \rho^2 + r_2^2 + \mu r_2 r_T \geq 0 \\ v_{N1} \geq 0 \Rightarrow r_2 + \mu r_T \leq 0 \Rightarrow \eta_1 \leq 1, \text{ and} \\ v_{TL2} \geq 0 \Rightarrow \frac{\gamma_T^-}{\gamma_N^-} \geq (1+\varepsilon_N) \frac{\mu(\rho^2 + r_T^2) + r_2 r_T}{\rho^2 + r_2^2 + \mu r_2 r_T} \end{cases} \quad (52)$$

V. *Backward slip at the acute corner*

In the case of backward slip at the acute corner ($\Lambda_{N1} > 0$, $\Lambda_{N2} = 0$, and $\Lambda_{T1} = +\mu\Lambda_{N1}$) the existential conditions are derived, following the same reasoning, as:

$$\begin{cases} \Lambda_{N1} \geq 0 \Rightarrow \mu r_1 r_T + r_1^2 + \rho^2 \geq 0 \\ v_{N2} \geq 0 \Rightarrow (r_1 + \mu r_T)(r_1 - r_2) \leq 0 \end{cases} \quad (53)$$

It is interesting to note that condition $v_{N2} \geq 0$ results in a contradiction, since both $r_1 - r_2 > 0$ and $r_1 + \mu r_T > 0$ are positive. Hence, single backward slip cannot take place at the acute corner of a skew rigid body, a conclusion not so intuitive.

VI. *Forward slip at the obtuse corner*

Similarly to backward slip at the obtuse corner, forward slip at the obtuse corner ($\Lambda_{N2} > 0$, $\Lambda_{N1} = 0$, and $\Lambda_{T2} = -\mu\Lambda_{N2}$) results in:

$$\left\{ \begin{array}{l} \frac{\Lambda_{N2}}{m\gamma_N^-} = -\frac{(1+\varepsilon_N)}{1+\frac{r_2^2-\mu r_2 r_T}{\rho^2}} \\ \frac{\gamma_{N1}^+}{\gamma_N^-} = 1 - (1+\varepsilon_N) \frac{\rho^2+r_1 r_2-\mu r_1 r_T}{\rho^2+r_2^2-\mu r_2 r_T} \end{array} \right. \quad (54)$$

with the pertinent existential conditions given by:

$$\left\{ \begin{array}{l} v_{N1} \geq 0 \Rightarrow r_2 - \mu r_T \geq 0 \Rightarrow \eta_1 \leq 1 \\ \Lambda_{N2} \geq 0 \Rightarrow \rho^2 + r_2^2 - \mu r_2 r_T \geq 0 \end{array} \right. , \text{ and} \quad (55)$$

$$v_{TR2} \geq 0 \Rightarrow \frac{\gamma_T^-}{\gamma_N^-} \leq \frac{r_2 r_T - \mu(r_T^2 + \rho^2)}{\rho^2 + r_2^2 - \mu r_2 r_T} (1 + \varepsilon_N)$$

VII. *Forward slip at the acute corner*

Forward slip at the acute corner is described by Equations (54 and 55) substituting lever r_2 with lever r_1 (with the exception of product $r_1 r_2$ which remains as it is).

VIII. *Stick at the obtuse corner*

Impulses in the normal and the transversal direction for stick at the obtuse corner ($A_{N2} > 0$, $A_{N1} = 0$, and $|\Lambda_{T2}| < \mu \Lambda_{N2}$) are calculated from Equations (9) and (10) with the help of the complementarity conditions (12) as:

$$\frac{\Lambda_{N2}}{m\gamma_N^-} = \frac{-(\rho^2 + r_T^2)(1 + \varepsilon_N) + r_2 r_T (1 + \varepsilon_T) \frac{\gamma_T^-}{\gamma_N^-}}{\rho^2 + r_2^2 + r_T^2} \quad (56)$$

$$\frac{\Lambda_{T2}}{m\gamma_N^-} = \frac{r_2 r_T (1 + \varepsilon_N) - (\rho^2 + r_2^2)(1 + \varepsilon_T) \frac{\gamma_T^-}{\gamma_N^-}}{\rho^2 + r_2^2 + r_T^2}$$

the existential conditions for stick at the obtuse corner are:

$$\frac{\gamma_T^-}{\gamma_N^-} < \frac{\rho^2 + r_T^2}{r_2 r_T} \frac{1 + \varepsilon_N}{1 + \varepsilon_T}$$

$$\left(\rho^2 + r_2^2 - \mu r_2 r_T \right) \frac{\gamma_T^-}{\gamma_N^-} > \left[r_2 r_T - \mu (\rho^2 + r_T^2) \right] \frac{1 + \varepsilon_N}{1 + \varepsilon_T} \quad (57)$$

$$\left(\rho^2 + r_2^2 + \mu r_2 r_T \right) \frac{\gamma_T^-}{\gamma_N^-} < \left[r_2 r_T + \mu (\rho^2 + r_T^2) \right] \frac{1 + \varepsilon_N}{1 + \varepsilon_T}$$

IX. *Stick at the acute corner*

For (single) stick at the acute corner Equations (56 and 57) hold where in lieu of lever r_2 , lever r_1 is used.

The combinations of the LCP (11) with transversal impulses of opposite sign (at the two impacts) lack physical interpretation. If for instance $\lambda_{T1} = +\mu\lambda_{N1}$ and $\lambda_{T2} = -\mu\lambda_{N2}$ the complementarity conditions (12) yield: $v_{TL1} \geq 0$ and $v_{TR2} \geq 0$.

5.2 Synopsis

The synopsis of all physically feasible combinations of the LCP (11) shows that the response of the examined oblique frictional multi-impact is mainly determined by two criteria: the first criterion is the transversal and the normal velocity ratio γ_T^- / γ_N^- which determines whether the double impact is forward/backward slip or stick. The second criterion is the dimensionless geometrical ratio (η_0) proposed for frictionless impact or the pertinent ratios of frictional impact ($\eta_{1,2}$), given by:

$$\eta_{1,2} = \eta_0 \left(1 \pm \frac{\mu}{\tan a} \right) = \frac{\sin 2a}{2(W/L)} \left(1 \pm \frac{\mu}{\tan a} \right) \quad (58)$$

where sign (+) holds for backward slip (η_1) and sign (-) for forward slip (η_2).

In Figure 10 the critical curves for both backward ($\eta_1=1$) and forward slip ($\eta_2=\pm 1$) are illustrated for a given coefficient of friction $\mu = 0.5$ (top) and $\mu = 1.0$ (bottom). Points B1, B2 and B3 correspond to skew bridges with increasing skew ratios η_0 (see also Figure 11). The proposed criteria $\eta_{1,2}$ (Equations 58) distinguish the double-impact response of a skew body into two distinct types: for $\eta_1 \leq 1$ (backward slip) or $|\eta_2| \leq 1$ (forward slip), double frictional impact results in zero angular velocity and hence zero rotation of the body, otherwise double impact produces angular velocity and hence rotation. Subsequently, the critical curves ($\eta_1=1, \eta_2=\pm 1$) of Figure 10 (and Figure 12 later on) divide the plane ($W/L, \alpha$) of skew bodies, depending on the assumed coefficient of friction (μ), into two areas: the one above the pertinent curves wherein $\eta_1 < 1$ (or $-1 < \eta_2 < 1$) holds and the area below the pertinent curves wherein $\eta_1 > 1$ (or $\eta_2 > 1, \eta_2 < -1$) holds. Note that double stick is feasible in the grey areas of Figure 10 provided the transversal - normal velocity ratio γ_T^- / γ_N^- is low enough:

$$\left| \gamma_T^- / \gamma_N^- \right| \leq (1 + \varepsilon_N) \mu .$$

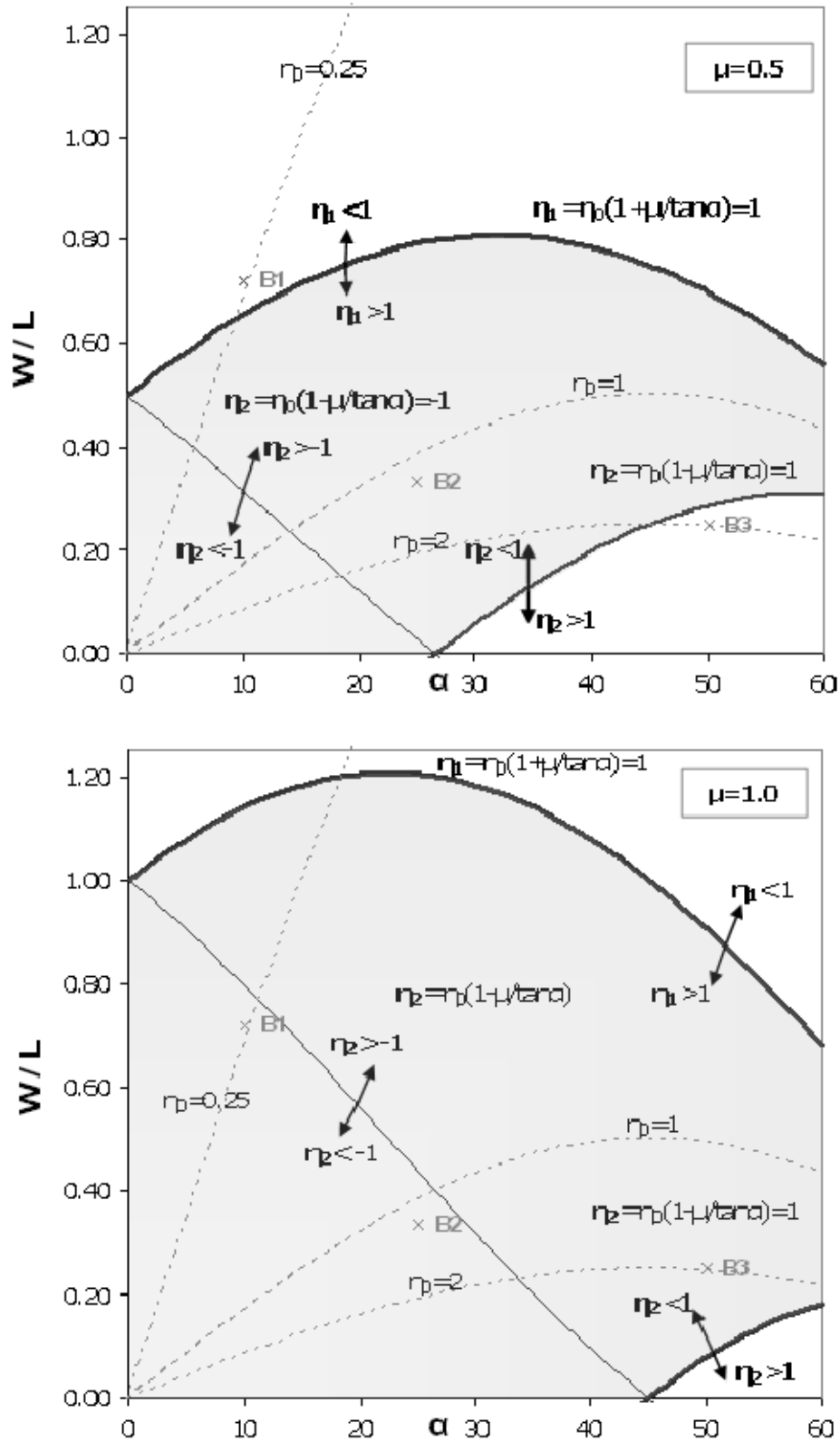


Figure 10. Critical curves $\eta_0=1$, $\eta_1=1$, $\eta_2=\pm 1$ in the plane Width/Length (W/L) – Skew angle (α), for friction coefficient $\mu=0.5$ (top) and $\mu=1.0$ (bottom).

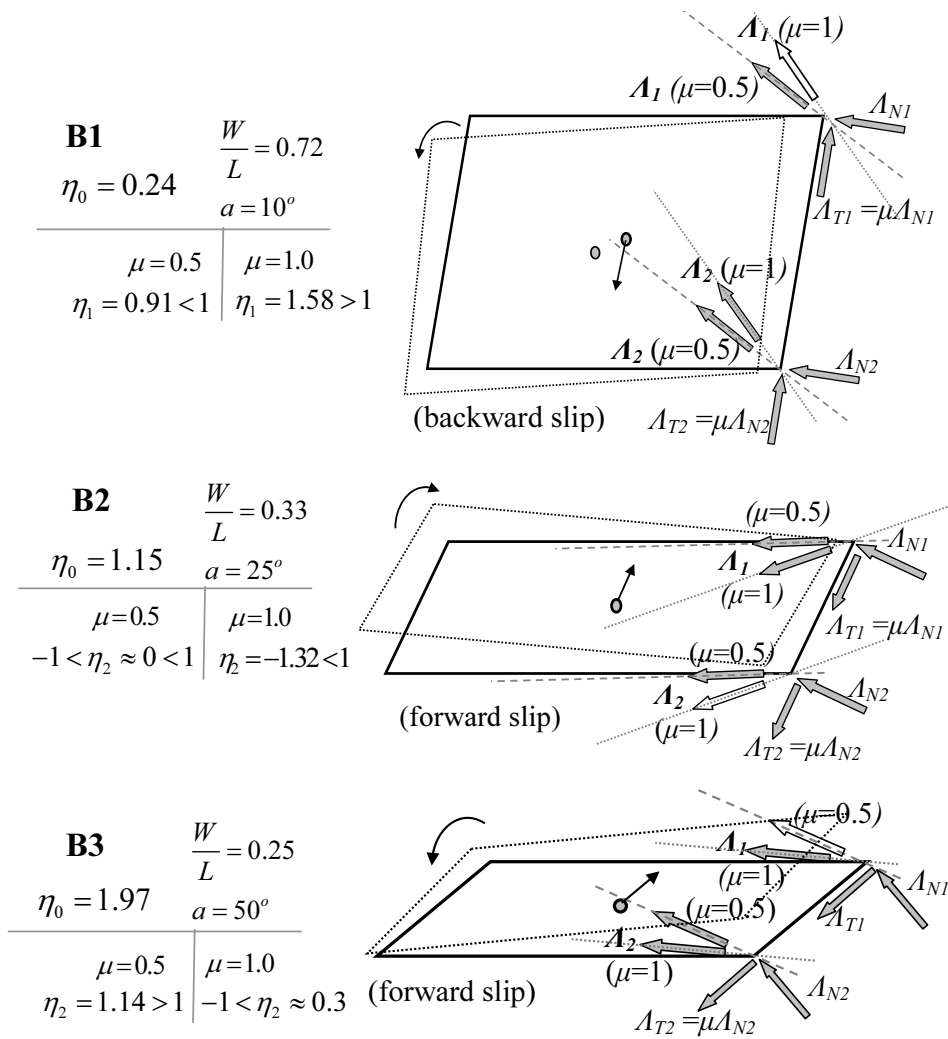


Figure 11. The double impact of three bridge decks (B1, B2, B3) with increasing dimensionless skew ratios η_0 for two coefficients of friction. Top: backward slip, middle and bottom: forward slip. Dashed lines indicate a feasible post-impact position.

Figure 10 illustrates that for $\mu = 0$ bridges with modest and high dimensionless skew ratios η_0 (e.g. points B2 and B3 accordingly) rotate 5 after backward slip. On the contrary bridges with small dimensionless skew ratios η_0 (e.g. point B1) do not rotate after backward slip. As μ increases (Figure 10 bottom, $\mu = 1.0$) so does the tendency of skew bridges to rotate since all three points (B1, B2 and B3) are below the curve $n_1 = 1$ which means that bridges of a wide range of dimensionless skew ratios η_0 rotate, after double backward slip, in such a way that the skew angle increases in accordance with the relevant literature [5]. Figure 10 also shows that after double forward slip only bridges with high η_0 (e.g. B3) rotate, provided the coefficient of friction μ is not high, resulting in increasing the skew angle ($n_2 > 1$). A counter-intuitive rotation which results in decreasing the skew angle, appears after forward slip for small and modest

dimensionless skew ratios η_0 (e.g. points B1 and B2) when the coefficients of friction is high ($\eta_2 > -1$, see also Figure 11 middle).

Figure 11 illustrates the geometry of the rotational mechanism associated with double frictional impact, which is similar to the frictionless case. When the angular momentums of the resultant impulses are in different directions with respect to the centre of mass (C.M.) the angular momentums cancel out and no rotation is developed. On the contrary, when the angular momentums are in the same direction angular velocity and hence rotation is developed. The white arrows in Figure 11 present impacts that must be ignored since they violate the inequality constraint $A_N \geq 0$. As Figure 11 unveils, the areas wherein $\eta_1 > 1$ and $\eta_2 > 1$ hold, correspond to rotation, after double backward and forward slip (impact) accordingly, in the direction of increasing the skew angle. This trend is in agreement with the relevant literature [5]. On the contrary, the area wherein $\eta_2 < -1$ holds corresponds to rotation, after double forward slip, in the (opposite) direction of decreasing the skew angle. This counter-intuitive rotation is not mentioned in earthquake engineering literature.

Figure 12 presents the critical curves of the proposed criteria for backward slip ($\eta_1 = 1$, Figure 12 top), forward slip ($\eta_2 = \pm 1$, Figure 12 bottom) and different coefficients of friction μ . The frictionless case analyzed in the previous section is captured with the $\mu = 0$ curve ($\eta_0 = 1$). Figure 12 shows that most skew bodies tend to rotate after backward slip and not after forward slip since the area wherein $\eta_1 > 1$ holds is broader than that of $\eta_2 > 1$ or $\eta_2 < -1$. As μ increases, the tendency towards rotation in the direction of increasing the skew angle accentuates after backward slip ($\eta_1 > 1$) but diminishes after forward slip ($\eta_2 > 1$). On the other hand, as μ increases the counter-intuitive rotation, in the direction of decreasing the skew angle ($\eta_2 < -1$), becomes feasible after forward slip. This counter-intuitive behaviour is more pronounced for small dimensionless skew ratios η_0 . It is noted though, that for a specific skew bridge (a specific point in the $W/L - \alpha$ plane) and a given coefficient of restitution, only one of the directions of rotation is feasible to occur after forward slip. In other words the two trends do not coexist.

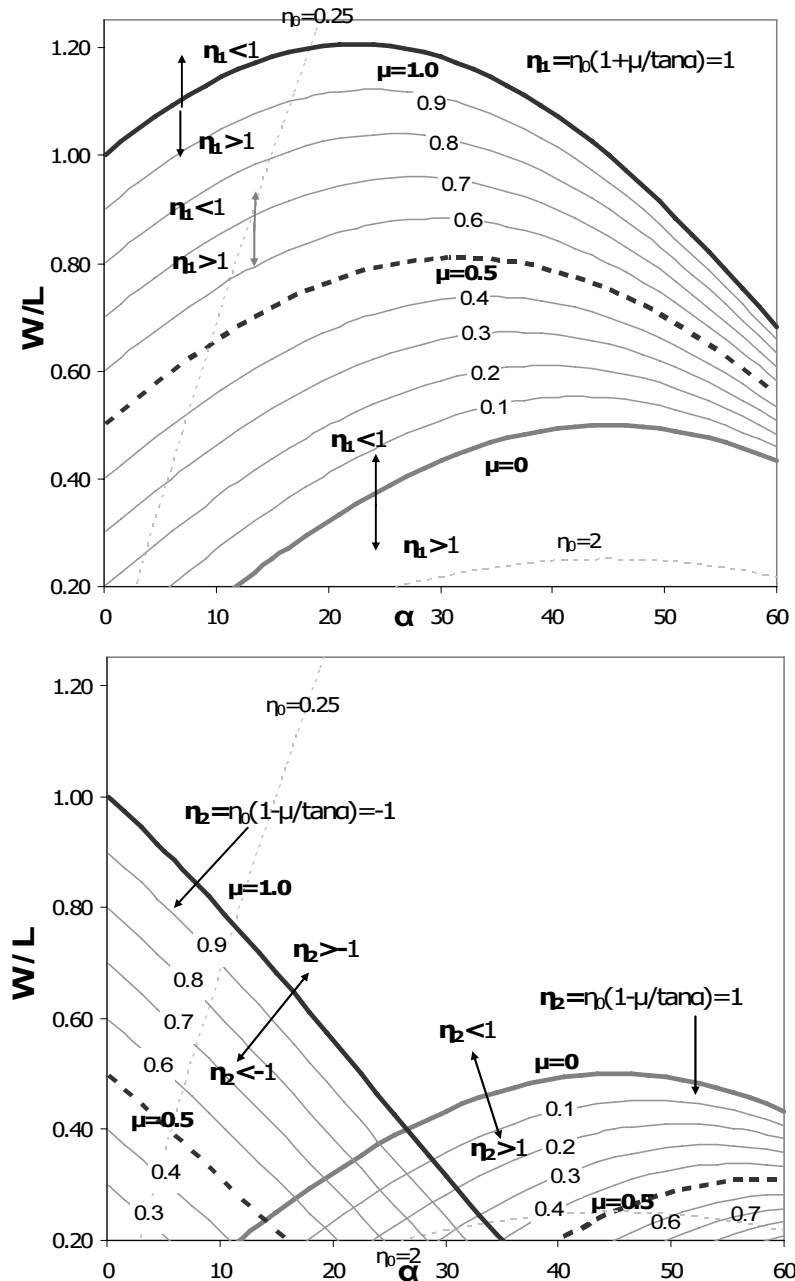


Figure 12. Critical curves of the proposed criteria $\eta_{1,2}$, in the plane Width/Length (W/L) – Skew angle (α), for different coefficients of friction μ . Top: double backward slip, bottom: double forward slip

5.3 Single frictional impact

Single-impacts occur when contact takes place at one corner of the rigid body (Figure 5 left), i.e. when $\theta^- \neq 0$ and/or $u_{\theta}^- \neq 0$. Within the context of this paper however, single frictional impacts can be considered as a special case of the double-impact analysed in the previous section. Each double impact for which $A_N = 0$ holds at one of the impact points, is in essence a single impact at the closed impact point ($A_N >$

0). Hence, using the appropriate lever arms either of the acute $(\tilde{r}_{N1}, \tilde{r}_{T1})$ or of the obtuse corner $(\tilde{r}_{N2}, \tilde{r}_{T2})$ all physically feasible single impacts can be described also with the LCP (11). For example, backward slip at the obtuse corner is described by Equations (51) and existential conditions (Equation 52), where instead of r_2 and r_T , \tilde{r}_{N2} and \tilde{r}_{T2} are used. This can be shown also with the comparison of Equations (51 to 57) with the pertinent relations of Payr & Glocker [16] derived from a similar LCP which treats single frictional impacts.

Figures 13 to 15 illustrate the existential conditions of the three different single-frictional-impact states (forward slip $A_T = -\mu A_N$, backward slip $A_T = +\mu A_N$ and stick $|A_T| < \mu A_N$) in the plane: pre-impact transversal and normal velocity ratio $(\gamma_T^- / \gamma_N^-)$ – pre-impact rotation (θ) . Figure 14 concerns straight bridges i.e. with zero skew angle $\alpha = 0$. Due to the symmetry of the system the response is also symmetrical with respect to rotation. As expected, for frictionless collisions no stick (grey area of Figures 13 to 15) is observed, whereas as coefficient of friction μ increases the stick area becomes broader. Not so intuitive though, is that the same trend appears as the coefficient of restitution increases.

Figures 14 and 15 present the existential conditions of the three distinct (single) impact states, for different skew angles α . For positive pre-impact rotations $\theta > 0$ impact occurs at the obtuse corner, while for negative rotations $\theta < 0$ impact occurs at the acute corner. In bridges the range of rotation values with practical significance is of the order of a few degrees. Within that range, the stick area is systematically broader for (small) positive rotations than it is for (small) negative rotations. This observation is in agreement with the qualitative remarks, found in the literature, that skew bridges tend to jam at the obtuse corner [5]. As the skew angle (α) increases the system becomes less symmetrical and similarly less symmetrical becomes its response with respect to (pre-impact) rotations θ . It is also interesting to note that the tendency to stick becomes more pronounced as the skew angle α becomes smaller.

In Figure 14 (bottom right) for skew angle $\alpha = 30^\circ$, coefficient of friction $\mu = 1.0$ and pre-impact rotations $\theta < -20^\circ$ only two impact states are feasible, backward slip and stick (at the acute corner). In other words, the third impact state, in this case forward slip, is not feasible. This phenomenon is due to the Painlevé paradox [14] which emerges when a critical maximal coefficient of friction is exceeded. However,

a detailed discussion on the Painlevé paradox is beyond the scope of this paper which is oriented towards results applicable to bridges, where (pre-impact) rotations remain within the range of a few degrees.

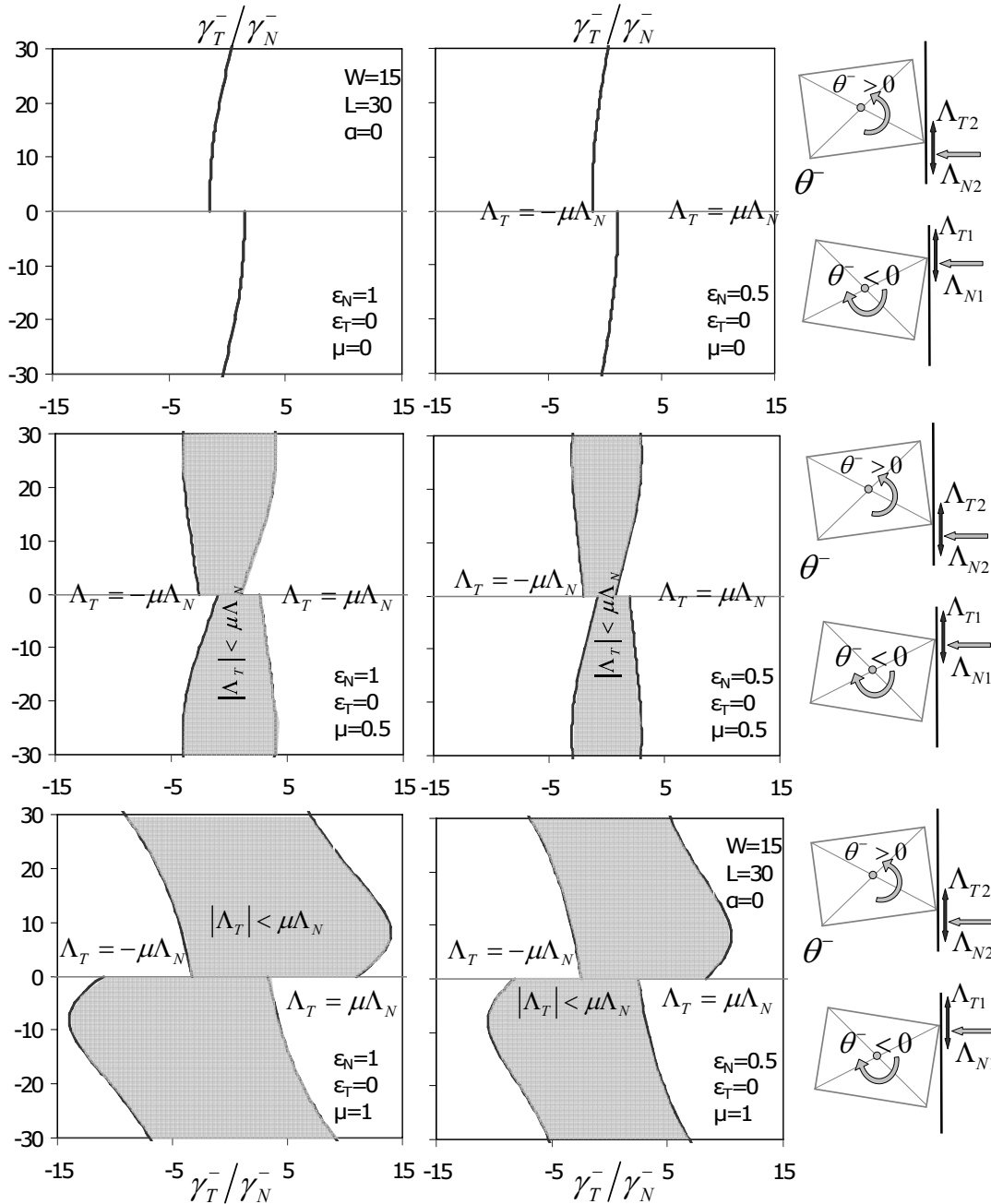


Figure 13. The three distinct single frictional impact states in the $(\gamma_T^-/\gamma_N^- - \theta^-)$ plane for straight bridges (zero skew angle $\alpha = 0$). Coefficient of restitution $\epsilon_N = 1.0$ (left), 0.5 (right), coefficient of friction $\mu = 0$ (top), 0.5 (middle) and 1.0 (bottom).

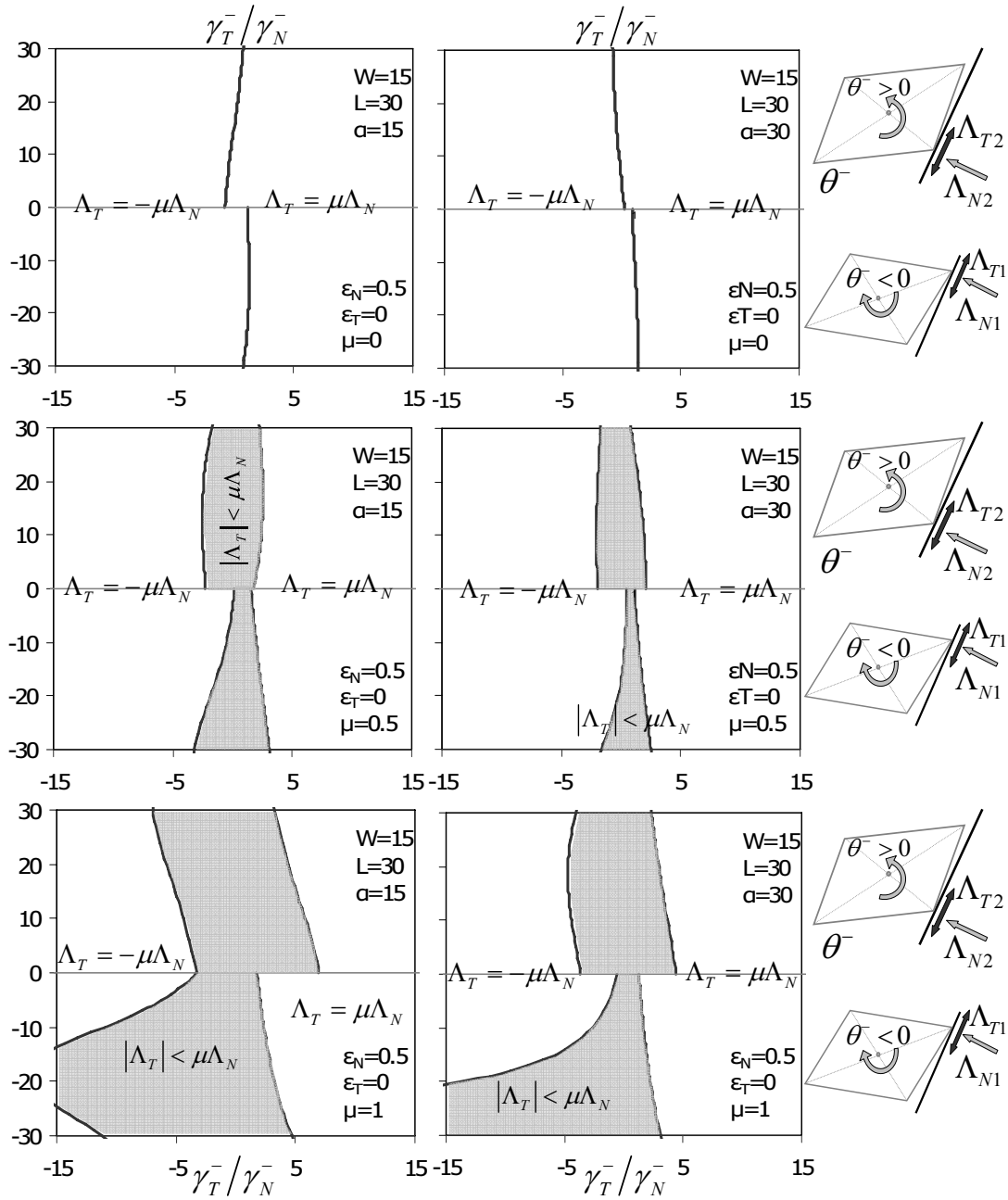


Figure 14. The three distinct single frictional impact states in the $(\gamma_T^-/\gamma_N^- - \theta^-)$ plane for coefficient of restitution $\epsilon_N = 0.5$. Skew angle $\alpha = 15^\circ$ (left), 30° (right), coefficient of friction $\mu = 0$ (top), 0.5 (middle) and 1.0 (bottom).

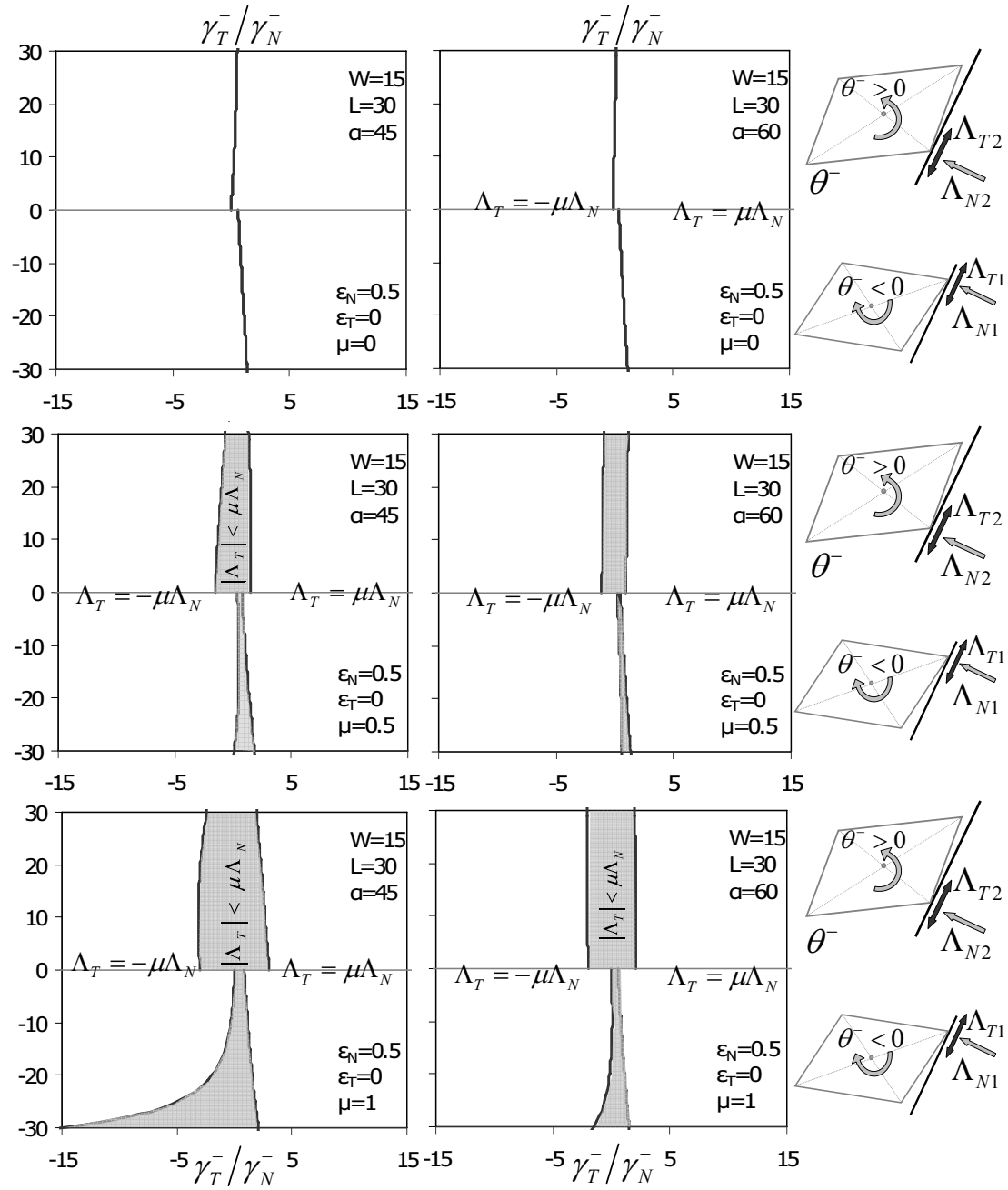


Figure 15. The three distinct single frictional impact states in the $\gamma_T^-/\gamma_N^- , \theta^-$ plane for coefficient of restitution $\epsilon_N= 0.5$. Skew angle $\alpha =45^\circ$ (left), 60° (right), coefficient of friction $\mu = 0$ (top), 0.5 (middle) and 1.0 (bottom).

Conclusions

The aim of the present paper is to bring forward the physical mechanism behind deck-abutment collisions in skew bridges. The relevant literature lacks a thorough theoretical study and is mostly confined to empirical descriptions of the phenomenon. Building on the work of other researchers, the study adopts a fully non-smooth rigid

body approach and examines in depth the impact response of a planar skew (rigid) body against an inelastic half-space, which encapsulates a lot of the ‘physics’ involved in deck-abutment collisions.

The study unveils the rotational mechanism associated with (double) oblique impact and shows that the tendency of skew bridges to rotate depends on the total geometry of the body in plan, not on the skew angle alone, in contrast to what is commonly considered in empirical vulnerability methodologies for bridges. Double oblique impact, either frictionless or frictional, triggers rotation when the resultant impulses of the two impact points produce angular momentums in the same direction with respect to the centre of mass. The study also concludes that skew bridges prefer to rotate in such a way that the skew angle increases, in agreement with the relevant literature. However, a counter-intuitive rotation in the opposite direction of decreasing the skew angle, which is caused by friction is also unveiled.

Frictional oblique impact is treated via a linear complementarity formulation, which includes single impacts as a special case of the examined double oblique impact. The physically feasible impact states are determined, the pertinent existential conditions are derived and specific criteria are proposed that determine whether double-impact triggers rotation. The present analysis finally examines the effect of the impact parameters (coefficient of restitution in the normal direction and coefficient of friction in the transversal direction) on the response and illustrates the complexity of the examined oblique impact.

Acknowledgements

The present paper is largely based on the doctoral thesis presented by the author to the Civil Engineering Department of the Aristotle University of Thessaloniki. The writer gratefully acknowledges the valuable contribution of the supervisors Prof. Andreas Kappos and Prof. Nicos Makris in shaping the ideas presented herein.

References

1. Dimitrakopoulos EG, Kappos AJ, Makris N. Dimensional Analysis of Yielding and Pounding Structures for Records Without Distinct Pulses. *Soil Dynamics Earthquake Engineering* 2009; 29(7): 1170-1180.
2. Dimitrakopoulos EG, Makris N, Kappos AJ. Dimensional Analysis of the Earthquake Response of a Pounding Oscillator. *Journal of Engineering Mechanics (ASCE)* submitted 2008;

3. Dimitrakopoulos EG, Makris N, Kappos AJ. Dimensional Analysis of the Earthquake Induced Pounding between Adjacent Structures. *Earthquake Engineering & Structural Dynamics* 2009; 38(7): 867-886
4. EERL (Earthquake Engineering Research Laboratory). Engineering features of the San Fernando earthquake of February 9, 1971 In: Jennings PC (ed) EERL 71-02 California Institute of Technology, Pasadena, Calif., 1971
5. Priestley MJN, Seible F, Calvi GM. Seismic design and retrofit of bridges. New York: Wiley, 1996
6. EERI. The Tehuacan, Mexico, Earthquake of June 15, 1999 Special Earthquake Rep. September 1999 EERI, Oakland, Calif, 1999
7. Kim SH. GIS-based Regional Risk Analysis Approach for Bridges Against Earthquakes Department of Civil Engineering, State University of New York at Buffalo 1993
8. Maragakis E, Jennings PC. Analytical Models for the Rigid Body Motions of Skew Bridges. *Earthquake Engineering and Structural Dynamics* 1987; 15: 923-944
9. Maleki S. Seismic Modeling of Skewed Bridges with Elastomeric Bearings and Side Retainers. *Journal of Bridge Engineering (ASCE)* 2005; 10 (4): 442-449
10. Moreau JJ. Unilateral contact and dry friction in finite freedom dynamics In: Moreau JJ Panagiotopoulos PD (eds) *Non-Smooth Mechanics and Applications*, Thessaloniki, Greece, pp 1-82, 1988
11. Panagiotopoulos PD. Dynamic and Incremental Variational Inequality Principles, Differential Inclusions and Their Applications to Co-Existent Phases Problems. *Acta Mechanica* 1981; 40: 85-107
12. Panagiotopoulos PD. Nonconvex Energy Functions. Hemivariational Inequalities and Substationary Principles. *Acta Mechanica* 1983; 48: 111-130
13. Glocker C. *Set-Valued Force Laws*. Springer, 2001
14. Brogliato B. *Nonsmooth Mechanics*. second edn. London: Springer, 1999
15. Leine RI, van Campen DH, Glocker C. Nonlinear Dynamics and Modeling of Various Wooden Toys with Impact and Friction. *Journal of Vibration and Control* 2003; 9: 25-78
16. Payr M, Glocker C. Oblique Frictional Impact of a Bar: Analysis and Comparison of Different Impact Laws. *Nonlinear Dynamics* 2005; 41: 361-383
17. Brogliato B, ten Dam AA, Paoli L, Ge'not F, Abadie M. Numerical simulation of finite dimensional multibody nonsmooth mechanical systems. *Appl. Mech. Rev. (ASME)* 2002; 55 (2): 107-150
18. Pfeiffer F, *Nonsmooth Dynamics in Engineering. Nonsmooth/Nonconvex Mechanics with Applications in Engineering, II*. NNMAE, Thessaloniki, Greece. 2006, 295-306
19. Kwack BM, Lee SS. A complementarity problem formulation for two-dimensional frictional contact problems. *Comput. Struct.* 1988, 28: 469-480.
20. Klarbring A, Bjrrkman G. A mathematical programming approach to contact problem with friction and varying contact surface. *Comput. Struct.* 1988, 30: 1185-1198.
21. Pfeiffer F, Glocker C. *Multibody Dynamics with Unilateral Contacts*. New York: Wiley, 1996